Layerwise mixed elements with node-dependent kinematics for global–local stress analysis of multilayered plates using high-order Legendre expansions

Layerwise mixed elements with node-dependent kinematics for global–local stress analysis of multilayered plates using high-order Legendre expansions

F. Moleiro[a,*], E. Carrera[b], E. Zappino[b], G. Li[b], M. Cinefra[b]

[a] *LAETA, IDMEC, Instituto Superior Técnico, Universidade de Lisboa, Av. Rovisco Pais 1, 1049-001 Lisboa, Portugal*
[b] *Politecnico di Torino, Corso Duca degli Abruzzi 24, 10129 Torino, Italy*

Abstract

Carrera Unified Formulation (CUF) is taken a step further to render node-dependent kinematics (NDK) capabilities to new layerwise finite elements based on Reissner's Mixed Variational Theorem (RMVT), especially suited for global–local stress analysis of multilayered plates, ensuring high numerical accuracy and computational efficiency, all together. In the framework of CUF, as introduced originally for multilayered structures, any degree of kinematic refinement can be considered in agreement with Equivalent Single-Layer (ESL) or Layer-Wise (LW) theories to develop advanced finite element models, whether based on the Principle of Virtual Displacements (PVD) or RMVT. The degree of kinematic refinement, which usually holds equally for the entire element, can be taken a step further, by being assigned locally to each of its nodes, making full use of CUF to render NDK capabilities to the elements. Besides, even though the elements can adopt any type of nodal shape functions, high p-order hierarchical Legendre expansions (HLE) can also be combined with NDK, achieving excellent convergence rates. These capabilities combined, explored first under the PVD, are for once integrated in the proposed elements under RMVT to further benefit accurate stress analysis. These elements can be applied throughout the entire mesh, adapting to local, transitional and global regions straightforwardly, providing high numerical accuracy, locally, with minimal computational efforts, globally. The numerical results focus on stress analysis of multilayered composite plates, including local effects, to demonstrate the predictive capabilities of the proposed RMVT-based LW elements with NDK and HLE combined, considering well-known benchmark three-dimensional exact solutions for assessment.

Keywords: Carrera Unified Formulation, Layerwise mixed models, Node-dependent kinematics, Legendre polynomials, Multilayered composite plates.

1. Introduction

Structural design technology nowadays relies, more and more, on the ever-growing potential of multilayered composite structures driven by the advances of composite materials science. In leading-edge engineering applications, multilayered composite structures are now, more than ever, subjected to extreme loading conditions and severe environments. This poses challenging demands to finite element analysis of multilayered composite structures, pushing forward the modelling predictive capabilities to capture complicated local effects that may be exhibited, with high numerical accuracy, all along maintaining fast, computational efficient techniques.

The modelling of multilayered composite structures, over the years, evolved mostly by accompanying the development of suitable theories for laminated composite beams, plates and shells, namely, early on, Equivalent-Single Layer (ESL) theories, from the simple Classical Lamination Plate Theory (CLPT) to the Higher-order Shear Deformation Theories (HSDT), and later on, the more refined Layer-Wise (LW) theories. Over time, comprehensive assessments on the main theories and finite element models for multilayered composite structures became available, including leading reviews by Reddy and Robbins [1] and also Noor and Burton [2], the well-known book of Reddy [3], as well as a two part series of papers by Carrera [4, 5]. In fact, these two works introduce Carrera Unified Formulation (CUF) to develop multilayered plate and shell models, which can incorporate any degree of kinematic refinement, in agreement with either ESL or LW theories, by making use of sets of approximation functions through-thickness, in a unified compact form. Moreover, the importance of thermal stress analysis and the growth of smart composite structures technology motivated further advances on coupled multi-field modelling of multilayered composite structures. Some noteworthy assessments came to light as well, including fundamental reviews on thermo-elastic modelling by Noor and Burton [6] and also Tang et al. [7],

*Corresponding author
Email addresses: filipa.moleiro@tecnico.ulisboa.pt (F. Moleiro), erasmo.carrera@polito.it (E. Carrera), enrico.zappino@polito.it (E. Zappino), guohong.li@polito.it (G. Li), maria.cinefra@polito.it (M. Cinefra)

in addition to primary reviews on electro-elastic modelling by Saravanos and Heyliger [8] and Benjeddou [9]. Actually, the main theories and finite element models for coupled multi-field analysis of multilayered structures are also described in the framework of CUF in a recent, rather comprehensive book by Carrera et al. [10].

Overall, the most widespread finite element models for all type of structures are based on the Principle of Virtual Displacements (PVD), also denoted as displacement-based or classical formulations. Nonetheless, an accurate modelling of multilayered structures, in particular, requires the fulfilment of interlaminar C^0 continuity of both displacements and transverse stresses, due to compatibility and equilibrium reasons. As emphasized early on by Carrera [11], these so-called C_z^0 requirements can be fully fulfilled *a priori* through Reissner's Mixed Variational Theorem (RMVT) as an alternative to develop finite element models most suited for multilayered structures. In fact, the added benefit of RMVT is brought to light ever since CUF is introduced to develop models for multilayered structures based on either the two alternative variational statements, PVD or RMVT. In the framework of CUF, systematic assessments of displacement-based and mixed models for multilayered plates and shells, whether considering ESL or LW theories, are since then addressed in many works by Carrera et al. [12–14]. The usefulness of CUF continues to be demonstrated in recent works. Specifically, Cinefra et al. [15, 16] focused on hygrothermal analysis of multilayered plates and shells, using CUF under the PVD for assessment of various models with different kinematic assumptions. In addition, de Miguel et al. [17] considered CUF under RMVT, instead, for an accurate stress analysis of multilayered beams with general cross-section. In this work, in particular, the beam cross-section is mapped by adopting high p-order (two-dimensional) hierarchical Legendre expansions (HLE). These type of hierarchical shape functions are derived from the pioneer works by Babuška et al. [18] and Szabó et al. [19] on the p-version refinement approach of the finite element method, as also addressed in the fundamental book of Szabó and Babuška [20]. Actually, CUF combined with such (two-dimensional) HLE are first used by Pagani et al. [21] and Carrera et al. [22] to develop beam and plate models with high accuracy capabilities, revealing the numerical efficiency of these HLE.

Furthermore, recognizing the adequacy of mixed formulations for an accurate modelling of multilayered structures, as highlighted in leading works by Carrera et al. [11–14], an alternative approach is also proposed in a series of works by Moleiro et al. [23–28] considering LW theories to develop finite element models for multilayered composite plates based on least-squares variational principle combined with mixed formulations. All together, the LW mixed least-squares models developed by Moleiro et al. [23–28] focused step-by-step on pure mechanical, electro-mechanical, thermo-mechanical and hygro-thermo-mechanical analyses of multilayered composite plates, addressing embedded functionally graded material layers as well, in the more recent works. In fact, these models also take advantage of high p-order shape functions based on Legendre polynomials, in line with the work by Warburton et al. [29] on high-order shape functions, both hierarchical and nodal. Specifically, high p-order nodal shape functions defined in terms of Legendre polynomials are adopted by these LW mixed least-squares models, both in-plane and through-thickness, which are simply C^0 interpolant polynomials of Gauss–Lobatto–Legendre quadrature points. Ultimately, the models derived in this alternative framework, using such high-order shape functions, also demonstrate high accuracy capabilities and are even shown to be insensitive to shear locking. However, highly accurate models are still much dependent on quite demanding computational efforts.

In finite element analysis, over many years, different refinement approaches came to light to improve the numerical accuracy as necessary to capture complicated local effects, especially stress-related issues. The most standard approaches are based on adjusting the h-size of the mesh or the p-order of the shape functions, referred to as h-version or p-version of the finite element method, in addition to the hp-version as a combination of both. In these well established refinement approaches the kinematic assumptions hold equally for the entire finite element model and throughout the mesh. Hence, the pursuit of breakthrough approaches to combine different kinematics continues to motivate much research, leading to many interesting contributions thus far. In multiple model approaches, kinematically inconsistent models are combined for global–local analysis, namely, the sequential or multisteps methods, or instead, the simultaneous methods. These last methods, in particular, are characterized by a simultaneous analysis of the entire domain, where different finite element models are applied separately in different subregions, and compatibility is then enforced in the interfacial or overlapping zones. The simultaneous multiple model methods are thus directly extendible to nonlinear analysis. In fact, early on Fish [30] proposed the s-version of the finite element method to improve the accuracy in local subregions, by superimposing additional elements with higher-order kinematics on the global model, along with homogeneous boundary conditions on the superimposed displacement field to guarantee continuity. Actually, the s-version of the finite element method can also be used in combination with the h-version and p-version approaches, at the same time, as also addressed by Reddy [3]. Another procedure to develop simultaneous multiple model methods is the use of Lagrange multipliers, which are introduced in the variational statement by additional integrals to enforce compatibility between subregions. In particular, Blanco et al. [31, 32] derived an extended variational formulation to properly address kinematically incompatible models, whereas Dhia et al. [33] proposed the Arlequin method as an engineering design tool to handle the compatibility between superimposed zones. In fact, Arlequin method is employed by Biscani et al. [34, 35] to couple different models derived through CUF, which can conveniently incorporate any degree of kinematic refinement, as appropriate.

The concept of node-dependent kinematics (NDK) emerged, in fact, within the framework of CUF. The suitable

degree of kinematic refinement, which usually holds equally for the entire element, can be taken a step further, by being assigned locally to each of its nodes, making full use of CUF to render NDK capabilities to the elements. Besides, these elements can adopt any type of shape functions, not only nodal but also hierarchical, which ultimately spread somewhat NDK over the element domain. As a result, elements with NDK capabilities can be applied throughout the entire mesh, adjusting the degree of kinematic refinement locally on the desired nodes, as necessary, without changing the mesh itself, and are thus most suitable for global–local analysis, bypassing *ad hoc* procedures to couple kinematically different models. Actually, the technique of NDK came to light by Carrera et al. [36, 37] to render unique capabilities to beam elements, which facilitated kinematic assumptions to be continuously varied along the beam axis, as appropriate. Shortly after, Carrera et al. [38] and Zappino et al. [39, 40] extended this technique to develop plate elements with NDK capabilities, aimed for global–local analysis of multilayered plates. In fact, even though the plate elements initially developed with NDK adopted nodal Lagrange type shape functions, the use of high p-order HLE combined with NDK is also explored recently by Zappino et al. [40], demonstrating excellent convergence rates. Still, the beam and plate elements developed thus far with NDK capabilities are based on the PVD. In the present work, a further advancement is pursued by the added benefit of RMVT for an accurate stress analysis of multilayered structures. Specifically, CUF is used herein to render NDK capabilities to new LW plate elements based on RMVT, in combination with HLE numerical efficiency, thus especially suited for global–local stress analysis of multilayered plates. In light of such advanced framework, these elements can be applied throughout the entire mesh, adapting to local, transitional and global regions straightforwardly, providing high numerical accuracy, locally, with minimal computational efforts, globally. The numerical results presented herein focus on stress analysis of multilayered composite plates, including local effects, to demonstrate the predictive capabilities of the proposed RMVT-based LW elements with NDK and HLE combined, considering well-known benchmark three-dimensional (3D) exact solutions for assessment.

2. Mechanical problem fundamentals

Consider a multilayered plate of total thickness h and a rectangular planar geometry Ω_0 of dimensions $a \times b$, as shown in Fig. 1. The multilayered plate coordinate system (x, y, z) is such that the z-axis is taken positive upward from the mid-plane in the thickness direction. In addition, k is used to denote each layer individually, ranging from 1 to N_l, which is the total number of layers. Each layer is assumed to be an orthotropic material, in general, including for instance, a unidirectional fibre reinforced composite layer of any given orientation relative to the multilayered plate x-axis. In such a case, a layer material coordinate system (x_k, y_k, z_k) is involved as usual, which can be transformed into the multilayered plate coordinate system by a simple in-plane rotation, according to the composite layer orientation. See Reddy [3] for further details.

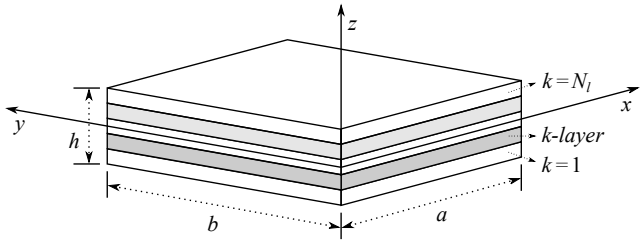

Figure 1: Geometry and coordinate system of a multilayered plate.

In essence, the mechanical problem concerning each k-layer individually in a LW approach, or the entire plate in an ESL approach, is much alike, as long as the same multilayered coordinate system is considered. Still, to be precise, the focus herein is on each k-layer, whose mechanical field variables can be conveniently arranged, all together, as follows:

$$\begin{aligned} &\boldsymbol{u}^k = \left\{u^k \;\; v^k \;\; w^k\right\}^{\mathsf{T}} \\ &\boldsymbol{\epsilon}_p^k = \left\{\varepsilon_{xx}^k \;\; \varepsilon_{yy}^k \;\; \gamma_{xy}^k\right\}^{\mathsf{T}}, \; \boldsymbol{\sigma}_p^k = \left\{\sigma_{xx}^k \;\; \sigma_{yy}^k \;\; \sigma_{xy}^k\right\}^{\mathsf{T}} \\ &\boldsymbol{\epsilon}_n^k = \left\{\varepsilon_{zz}^k \;\; \gamma_{xz}^k \;\; \gamma_{yz}^k\right\}^{\mathsf{T}}, \; \boldsymbol{\sigma}_n^k = \left\{\sigma_{zz}^k \;\; \sigma_{xz}^k \;\; \sigma_{yz}^k\right\}^{\mathsf{T}} \end{aligned} \tag{1}$$

where the subscripts p and n denote in-plane and out-of-plane components, respectively, for both strains and stresses.

2.1. Geometrical relations

Under the assumption of infinitesimal strains, the geometrical strain-displacement relations for each k-layer can then be expressed as shown:

$$\begin{aligned} \boldsymbol{\epsilon}_{pG}^{k} &= \boldsymbol{D}_{p}\boldsymbol{u}^{k} \\ \boldsymbol{\epsilon}_{nG}^{k} &= \left(\boldsymbol{D}_{np} + \boldsymbol{D}_{nz}\right)\boldsymbol{u}^{k} \end{aligned} \tag{2}$$

where the subscript G underlines that the vector field is derived from geometrical relations, in addition to the following differential operator matrices:

$$\boldsymbol{D}_{p} = \begin{bmatrix} \partial_x & 0 & 0 \\ 0 & \partial_y & 0 \\ \partial_y & \partial_x & 0 \end{bmatrix}, \; \boldsymbol{D}_{np} = \begin{bmatrix} 0 & 0 & 0 \\ 0 & 0 & \partial_x \\ 0 & 0 & \partial_y \end{bmatrix}, \; \boldsymbol{D}_{nz} = \begin{bmatrix} 0 & 0 & \partial_z \\ \partial_z & 0 & 0 \\ 0 & \partial_z & 0 \end{bmatrix} \tag{3}$$

using $\partial_{(\cdot)}$ to denote a partial derivative with respect to each spacial coordinate involved.

2.2. Constitutive relations

In agreement with linear elasticity, the constitutive relations considering infinitesimal strains, also referred to as the generalized Hooke's law, can be written in the multilayered plate coordinate system for each k-layer material, in standard contracted notation, as follows:

$$\boldsymbol{\sigma}^{k} = \bar{\boldsymbol{C}}^{k}\boldsymbol{\epsilon}^{k} \tag{4}$$

Note that even though each k-layer is assumed to be an orthotropic material, in the most general case, a prior in-plane rotation is necessary between the layer material coordinate system and the multilayered plate coordinate system. This is clearly indicated by the overbar in the material stiffness coefficients $\bar{C}_{ij}^{k}$, with $i, j = 1, \ldots, 6$, in line with the contracted notation, such that:

$$\begin{aligned} \boldsymbol{\epsilon}^{k} &= \left\{\varepsilon_{xx}^{k} \;\; \varepsilon_{yy}^{k} \;\; \varepsilon_{zz}^{k} \;\; \gamma_{yz}^{k} \;\; \gamma_{xz}^{k} \;\; \gamma_{xy}^{k}\right\}^{\intercal} \\ \boldsymbol{\sigma}^{k} &= \left\{\sigma_{xx}^{k} \;\; \sigma_{yy}^{k} \;\; \sigma_{zz}^{k} \;\; \sigma_{yz}^{k} \;\; \sigma_{xz}^{k} \;\; \sigma_{xy}^{k}\right\}^{\intercal} \end{aligned} \tag{5}$$

Rearranging the constitutive relations for each k-layer, considering in-plane and out-of-plane components separately, as before, leads then to:

$$\begin{aligned} \boldsymbol{\sigma}_{pH}^{k} &= \bar{\boldsymbol{C}}_{pp}^{k}\boldsymbol{\epsilon}_{pG}^{k} + \bar{\boldsymbol{C}}_{pn}^{k}\boldsymbol{\epsilon}_{nG}^{k} \\ \boldsymbol{\sigma}_{nH}^{k} &= \bar{\boldsymbol{C}}_{np}^{k}\boldsymbol{\epsilon}_{pG}^{k} + \bar{\boldsymbol{C}}_{nn}^{k}\boldsymbol{\epsilon}_{nG}^{k} \end{aligned} \tag{6}$$

where the subscript H underlines that the vector field is derived from Hooke's constitutive relations, together with the following stiffness matrices:

$$\begin{aligned} \bar{\boldsymbol{C}}_{pp}^{k} &= \begin{bmatrix} \bar{C}_{11}^{k} & \bar{C}_{12}^{k} & \bar{C}_{16}^{k} \\ \bar{C}_{12}^{k} & \bar{C}_{22}^{k} & \bar{C}_{26}^{k} \\ \bar{C}_{16}^{k} & \bar{C}_{26}^{k} & \bar{C}_{66}^{k} \end{bmatrix}, \; \bar{\boldsymbol{C}}_{pn}^{k} = \begin{bmatrix} \bar{C}_{13}^{k} & 0 & 0 \\ \bar{C}_{23}^{k} & 0 & 0 \\ \bar{C}_{36}^{k} & 0 & 0 \end{bmatrix} \\ \bar{\boldsymbol{C}}_{nn}^{k} &= \begin{bmatrix} \bar{C}_{33}^{k} & 0 & 0 \\ 0 & \bar{C}_{55}^{k} & \bar{C}_{45}^{k} \\ 0 & \bar{C}_{45}^{k} & \bar{C}_{44}^{k} \end{bmatrix}, \; \bar{\boldsymbol{C}}_{np}^{k} = \bar{\boldsymbol{C}}_{pn}^{k\,\intercal} \end{aligned} \tag{7}$$

In particular, all possible non-zero stiffness coefficients are here considered, assuming the most general case, in which a prior in-plane rotation is indeed necessary. For more detailed information, see Reddy [3].

2.3. Variational statements

In a variational framework, the static equilibrium of any general continuous body can be stated by the Principle of Virtual Displacements (PVD), establishing the equilibrium between the internal and external virtual work. Hence, the PVD for each k-layer can be conveniently expressed in the following form:

$$\int_{V} \left(\delta\boldsymbol{\epsilon}_{pG}^{k\,\intercal}\,\boldsymbol{\sigma}_{pH}^{k} + \delta\boldsymbol{\epsilon}_{nG}^{k\,\intercal}\,\boldsymbol{\sigma}_{nH}^{k}\right) \mathrm{d}V = \delta L_{ext}^{k} \tag{8}$$

where V denotes the layer volume and δL^k_{ext} stands for the layer external virtual work. To be more specific, considering in the layer boundary Γ an imposed surface load $\boldsymbol{p}^k$, the layer external virtual work can be further expressed as follows:

$$\delta L^k_{ext} = \int_\Gamma \delta \boldsymbol{u}^{k\intercal}\, \boldsymbol{p}^k \, \mathrm{d}\Gamma \tag{9}$$

In the end, the PVD is only based on the assumed displacement field, thus called a displacement-based formulation, as clearly understood by the subscripts involved in Eq. (8).

Alternatively, in view of Reissner's Mixed Variational Theorem (RMVT), both displacements and transverse stresses are assumed independently. Hence, RMVT for each k-layer can be simply derived by introducing additional constraint equations in the variational statement, associated with the transverse stresses, as follows:

$$\int_V \left[\delta \boldsymbol{\epsilon}^{k\intercal}_{pG}\, \boldsymbol{\sigma}^k_{pH} + \delta \boldsymbol{\epsilon}^{k\intercal}_{nG}\, \boldsymbol{\sigma}^k_{nM} + \delta \boldsymbol{\sigma}^{k\intercal}_{nM} \left(\boldsymbol{\epsilon}^k_{nG} - \boldsymbol{\epsilon}^k_{nH}\right)\right] \mathrm{d}V = \delta L^k_{ext} \tag{10}$$

where the subscript M underlines that the transverse stresses are here assumed in agreement with a mixed formulation. The third term, added in RMVT, variationally enforces the compatibility of the transverse strains derived independently from both geometrical and constitutive relations, as apparent by the subscripts involved in Eq. (10). In fact, the previous constitutive relations in Eq. (6) can be rearranged further, through a straightforward manipulation to take an alternative form, in terms of the (assumed) transverse stresses, as follows:

$$\begin{aligned} \boldsymbol{\sigma}^k_{pH} &= \hat{\boldsymbol{C}}^k_{pp} \boldsymbol{\epsilon}^k_{pG} + \hat{\boldsymbol{C}}^k_{pn} \boldsymbol{\sigma}^k_{nM} \\ \boldsymbol{\epsilon}^k_{nH} &= \hat{\boldsymbol{C}}^k_{np} \boldsymbol{\epsilon}^k_{pG} + \hat{\boldsymbol{C}}^k_{nn} \boldsymbol{\sigma}^k_{nM} \end{aligned} \tag{11}$$

where

$$\begin{aligned} \hat{\boldsymbol{C}}^k_{pp} &= \bar{\boldsymbol{C}}^k_{pp} - \bar{\boldsymbol{C}}^k_{pn} (\bar{\boldsymbol{C}}^k_{nn})^{-1} \bar{\boldsymbol{C}}^k_{np} \\ \hat{\boldsymbol{C}}^k_{pn} &= \bar{\boldsymbol{C}}^k_{pn} (\bar{\boldsymbol{C}}^k_{nn})^{-1} \\ \hat{\boldsymbol{C}}^k_{np} &= -(\bar{\boldsymbol{C}}^k_{nn})^{-1} \bar{\boldsymbol{C}}^k_{np} \\ \hat{\boldsymbol{C}}^k_{nn} &= (\bar{\boldsymbol{C}}^k_{nn})^{-1} \end{aligned} \tag{12}$$

Accordingly, in RMVT, vector fields with the subscript H are derived from the constitutive relations by this alternative form in Eq. (11), whereas vector fields with the subscript G are taken from the standard geometrical relations in Eq. (2). Moreover, all possible non-zero coefficients are also considered in the matrices in Eq. (12), as presented further in Appendix A, whose form is rather analogous to the previous matrices in Eq. (7).

3. Carrera Unified Formulation (CUF)

As introduced originally for two-dimensional (2D) modelling of multilayered structures, CUF can incorporate any degree of kinematic refinement, in agreement with either ESL or LW theories, by making use of sets of approximation functions through-thickness, in a unified compact form. For ESL models based on the PVD, the displacement field of a plate structure can be assumed in the framework of CUF, quite simply, in the following compact form:

$$\boldsymbol{u}(x,y,z) = F_\tau(z) \boldsymbol{u}_\tau(x,y), \quad \tau = 0, 1, \ldots, N \tag{13}$$

where $F_\tau(z)$ represents a set of (independent) approximation functions, also called thickness functions, which are defined through the thickness of the entire plate, i.e. $z \in [-\frac{h}{2}, \frac{h}{2}]$. In fact, N is considered a *free parameter* of the model, which determines the number of unknown primary variables, $\boldsymbol{u}_\tau(x,y)$, thus associated with the plate theory desired.

For LW models based on the PVD as well, the displacement field of each k-layer individually can also be assumed in the framework of CUF, rather analogously, in the following form:

$$\boldsymbol{u}^k(x,y,\zeta_k) = F^k_\tau(\zeta_k) \boldsymbol{u}^k_\tau(x,y), \quad \tau = 0, 1, \ldots, N^k \tag{14}$$

where $F^k_\tau(\zeta_k)$ are the so-called thickness functions of each k-layer, which are now defined through the layer thickness via the natural coordinate $\zeta_k \in [-1, 1]$. Similarly, N^k is considered a *free parameter* of the model, thus associated with the plate theory desired, but used instead for each k-layer individually, in line with a LW approach.

For LW models based on RMVT, both displacements and transverse stresses are assumed independently for each k-layer individually. Hence, in the framework of CUF both fields can be assumed similarly in the following form:

$$\begin{aligned} \boldsymbol{u}^k(x,y,\zeta_k) &= F^k_\tau(\zeta_k)\boldsymbol{u}^k_\tau(x,y) \\ \boldsymbol{\sigma}^k_n(x,y,\zeta_k) &= F^k_\tau(\zeta_k)\boldsymbol{\sigma}^k_{n\tau}(x,y), \quad \tau = 0,1,\ldots,N^k \end{aligned} \tag{15}$$

Most notably, N^k is still considered a *free parameter* of the model, which determines the number of unknown primary variables for each k-layer, namely, for RMVT-based LW models, all together $\boldsymbol{u}^k_\tau(x,y)$ and $\boldsymbol{\sigma}^k_{n\tau}(x,y)$, for each k-layer.

The adopted thickness functions can be selected from various expansions type of forms. In ESL models, one of the simplest forms for the adopted thickness functions is Taylor expansions, through the plate thickness, such that FSDT or HSDT theories can be readily considered, as shown:

$$F_0(z) = z^0 = 1,\ F_1(z) = z^1 = z,\ \ldots,\ F_N(z) = z^N \tag{16}$$

In LW models, whether displacement-based or mixed, the interlaminar C^0 continuity of the unknown primary variables is, in fact, ensured by the adopted thickness functions, wisely selected to fulfil this requirement *a priori*. Hence, one of the easiest forms for the adopted thickness functions is Lagrange expansions, through each layer thickness, in terms of the natural coordinate $\zeta_k \in [-1,1]$, as follows:

$$F^k_\tau(\zeta_k) = \prod_{\substack{s=0 \\ s\neq\tau}}^{N^k} \frac{\zeta_k - \zeta_{k\,s}}{\zeta_{k\,\tau} - \zeta_{k\,s}} \tag{17}$$

Alternatively, for an improved convergence rate, the use of high p-order Legendre polynomials L_p is actually most suitable for the adopted thickness functions, as proposed by Carrera [4, 5, 11] ever since the introduction of CUF. This type of Legendre expansions can be defined in terms of the natural coordinate $\zeta_k \in [-1,1]$, as suggested by Szabó et al. [19, 20], in the following form:

$$\begin{aligned} F^k_0(\zeta_k) &= \tfrac{1}{2}\left(L_0(\zeta_k) - L_1(\zeta_k)\right) = \tfrac{1}{2}\left(1 - \zeta_k\right) \\ F^k_1(\zeta_k) &= \tfrac{1}{2}\left(L_0(\zeta_k) + L_1(\zeta_k)\right) = \tfrac{1}{2}\left(1 + \zeta_k\right) \\ F^k_\tau(\zeta_k) &= \phi_p(\zeta_k), \quad \tau, p = 2,\ldots,N^k \end{aligned} \tag{18}$$

where

$$\phi_p(\zeta_k) = \tfrac{1}{\sqrt{4p-2}}\left(L_p(\zeta_k) - L_{p-2}(\zeta_k)\right), \quad p \geq 2 \tag{19}$$

Such thickness functions are, in fact, one-dimensional (1D) hierarchical Legendre expansions, which consist of *outer modes* and *interior modes*, as shown in Fig. 2. In the interest of numerical efficiency, the high p-order Legendre thickness functions as given by Eqs. (18)–(19) are indeed adopted by the new RMVT-based LW plate elements here proposed.

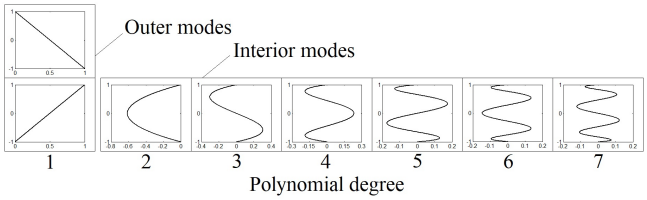

Figure 2: High p-order Legendre polynomials as thickness functions for each layer.

Most importantly, in RMVT-based LW models, in particular, considering that the unknown primary variables involve both displacements and transverse stresses, the so-called C^0_z requirements can, therefore, be fully fulfilled *a priori*, as follows:

$$\boldsymbol{u}^k_{(t)} = \boldsymbol{u}^{k+1}_{(b)},\ \boldsymbol{\sigma}^k_{n(t)} = \boldsymbol{\sigma}^{k+1}_{n(b)}, \quad k = 1,\ldots,N_l - 1 \tag{20}$$

where (t) and (b) denote the layer top and bottom surfaces, respectively. Actually, the C^0_z requirements are ensured quite simply by the assemblage process from layer to multilayer level, in line with a LW approach, as thoroughly described by Carrera and Demasi [12].

4. Hierarchical Legendre expansions (HLE)

For either ESL or LW models, displacement-based or mixed, finite element approximations are then used to express the unknown primary variables via shape functions. For 2D finite element models, in specific, the most commonly used shape functions, namely $N_i(x, y)$, are nodal 2D Lagrange type interpolation functions.

Nonetheless, 2D shape functions based on high p-order Legendre polynomials L_p, as originally proposed in the pioneer works by Babuška et al. [18] and Szabó et al. [19, 20] on the p-version of the finite element method, can also be used as an alternative, with an improved convergence rate. This type of shape functions are, in fact, 2D hierarchical Legendre expansions (HLE), which consist of *nodal modes*, *edge modes* and *surface modes*, as shown in Fig. 3.

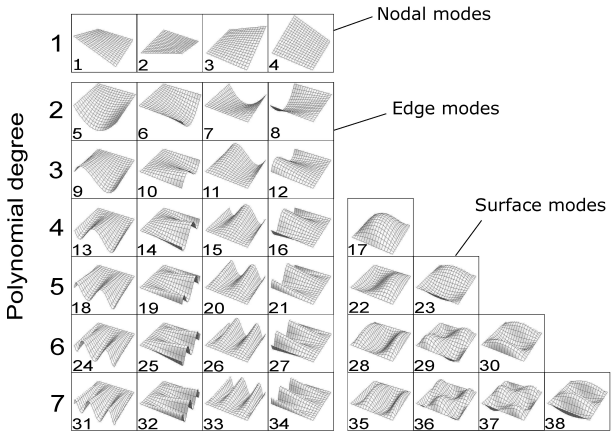

Figure 3: High p-order Legendre polynomials as shape functions for 2D finite elements.

Specifically, HLE are defined in terms of the natural coordinates $(\xi, \eta) \in [-1, 1]$, as follows:

Nodal modes

$$N_i(\xi, \eta) = \tfrac{1}{4}\left(1 - \xi_i \xi\right)\left(\eta_i \eta\right), \quad i = 1, 2, 3, 4 \tag{21}$$

Edge modes

$$\begin{aligned} N_i(\xi, \eta) &= \tfrac{1}{2}\left(1 - \eta\right)\phi_p(\xi), \quad i = 5, 9, 13, 18, \ldots \\ N_i(\xi, \eta) &= \tfrac{1}{2}\left(1 + \xi\right)\phi_p(\eta), \quad i = 6, 10, 14, 19, \ldots \\ N_i(\xi, \eta) &= \tfrac{1}{2}\left(1 + \eta\right)\phi_p(\xi), \quad i = 7, 11, 15, 20, \ldots \\ N_i(\xi, \eta) &= \tfrac{1}{2}\left(1 - \xi\right)\phi_p(\eta), \quad i = 8, 12, 16, 21, \ldots \end{aligned} \tag{22}$$

Surface modes

$$N_i(\xi, \eta) = \phi_m(\xi)\phi_n(\eta), \quad m, n \geq 2, \quad i = 17, 22, 23, 28, 29, 30, \ldots \tag{23}$$

where ϕ_p is given precisely according to the previous Eq. (19).

In fact, the high numerical efficiency of advanced beam and plate models benefiting from HLE is demonstrated by a series of recent works, including displacement-based models by Pagani et al. [21] and Carrera et al. [22], as well as mixed models by de Miguel et al. [17]. Most noteworthy, HLE is also shown most useful when combined with the latest technique of NDK, as explored recently by Zappino et al. [40] to develop quite efficient plate elements under the PVD. Thus, a further advancement is here pursued by the proposed RMVT-based LW plate elements with NDK capabilities, in combination with HLE numerical efficiency, according to Eqs. (21)–(23).

5. Node-dependent kinematics (NDK)

In the typical approach to develop 2D models in the framework of CUF, displacement-based or mixed, the assumed fields are defined in a unified compact form by making use of thickness functions, to incorporate any degree of kinematic refinement as desired, in line with ESL or LW theories, along with finite element approximations to express the unknown primary variables via 2D shape functions.

To be precise, in RMVT-based LW models, in particular, both displacements and transverse stresses are thus expressed as follows:

$$\begin{aligned}\boldsymbol{u}^k(x,y,\zeta_k) &= F^k_\tau(\zeta_k)N_i(x,y)\boldsymbol{u}^k_{\tau i}, \qquad i=1,\ldots,M\\ \boldsymbol{\sigma}^k_n(x,y,\zeta_k) &= F^k_\tau(\zeta_k)N_i(x,y)\boldsymbol{\sigma}^k_{n\tau i}, \quad \tau=0,1,\ldots,N^k\end{aligned} \tag{24}$$

where M is the total number of shape functions $N_i(x,y)$ per element, whereas N^k remains a *free parameter* of the model that also indicates the order of the adopted thickness functions $F^k_\tau(\zeta_k)$ for each k-layer. Therefore, in view of this typical approach to develop 2D models, the degree of kinematic refinement established by CUF holds equally for the entire element or, in other words, is invariant over the finite element model. The technique of NDK relies on a novel approach to develop the finite element, in which the degree of kinematic refinement can be taken a step further by being assigned locally to each of its nodes, making full use of CUF to render NDK capabilities to the elements. In fact, the degree of kinematic refinement established by CUF is, at its core, defined by the thickness functions, involving all together every k-layer in a LW approach. In short, the basic idea of NDK is to associate the thickness functions to each node i of the element, individually, rather than to the entire element itself.

According to this novel approach, to develop 2D RMVT-based LW elements with NDK capabilities, in specific, both displacements and stresses can still be expressed in compact form, as follows, making full use of CUF:

$$\begin{aligned}\boldsymbol{u}^k(x,y,\zeta_k) &= F^{ik}_\tau(\zeta_k)N_i(x,y)\boldsymbol{u}^k_{\tau i}, \qquad i=1,\ldots,M\\ \boldsymbol{\sigma}^k_n(x,y,\zeta_k) &= F^{ik}_\tau(\zeta_k)N_i(x,y)\boldsymbol{\sigma}^k_{n\tau i}, \quad \tau=0,1,\ldots,N^k\end{aligned} \tag{25}$$

where the underlying distinction lies in the thickness functions $F^{ik}_\tau(\zeta_k)$ now being assigned locally to each node i of the element, involving all together every k-layer in a LW approach. In practical terms, in an element with NDK capabilities, the i-local kinematics is ultimately spread somewhat over the finite element domain through the shape functions $N_i(x,y)$, providing a rather gradual effect among the i-local kinematics within the element. Moreover, these elements can adopt any type of shape functions, not only nodal but also hierarchical, as shown recently by Zappino et al. [39, 40], including most especially HLE.

Owing to this novel approach, elements with NDK capabilities can be applied throughout the entire mesh, adjusting the degree of kinematic refinement locally on the desired nodes, as necessary, without changing the mesh itself, bypassing *ad hoc* procedures to couple kinematically different models. Specifically, the proposed RMVT-based LW elements with NDK and HLE combined are thus especially suited for global–local stress analysis of multilayered plates, adapting to local, transitional and global regions straightforwardly, providing high numerical accuracy, locally, with minimal computational efforts, globally.

6. Finite element equations

The subsequent derivation of the new RMVT-based LW plate elements, including NDK capabilities, follows the usual finite element procedure, starting with the expression of the assumed field variables and their variations for each k-layer, in line with a LW approach, in compact form, as shown:

$$\begin{aligned}\boldsymbol{u}^k(x,y,\zeta_k) &= F^{ik}_\tau(\zeta_k)N_i(x,y)\boldsymbol{u}^k_{\tau i}, \qquad i=1,\ldots,M\\ \boldsymbol{\sigma}^k_{nM}(x,y,\zeta_k) &= F^{ik}_\tau(\zeta_k)N_i(x,y)\boldsymbol{\sigma}^k_{n\tau i}, \quad \tau=0,1,\ldots,N^k\end{aligned} \tag{26}$$

$$\begin{aligned}\delta\boldsymbol{u}^k(x,y,\zeta_k) &= F^{jk}_s(\zeta_k)N_j(x,y)\boldsymbol{u}^k_{sj}, \qquad j=1,\ldots,M\\ \delta\boldsymbol{\sigma}^k_{nM}(x,y,\zeta_k) &= F^{jk}_s(\zeta_k)N_j(x,y)\boldsymbol{\sigma}^k_{nsj}, \quad s=0,1,\ldots,N^k\end{aligned} \tag{27}$$

where, to be precise, the subscript M is included to underline the agreement with RMVT.

In fact, the geometrical and constitutive relations for each k-layer, addressed previously, can now be used to establish the layer strain and stress fields, as appropriate under RMVT. Moreover, considering the compact (vector) form set by Eqs. (26)–(27), to begin with, the identity matrix of size 3×3 is henceforth introduced when suitable for clearness.

To this end, first, the substitution of the assumed displacements in Eq. (26) into the geometrical relations, as given by Eq. (2), for each k-layer, leads to:

$$\begin{aligned}\boldsymbol{\epsilon}^k_{pG} &= \boldsymbol{D}_p(F^{ik}_\tau N_i\boldsymbol{I})\boldsymbol{u}^k_{\tau i}\\ \boldsymbol{\epsilon}^k_{nG} &= (\boldsymbol{D}_{np}+\boldsymbol{D}_{nz})\,(F^{ik}_\tau N_i\boldsymbol{I})\boldsymbol{u}^k_{\tau i}\end{aligned} \tag{28}$$

Secondly, the further substitution of the assumed transverse stresses in Eq. (26), as well as the in-plane strains just derived in Eq. (28), into the constitutive relations, as properly given by the alternative form in Eq. (11), for each k-layer, leads also to:

$$\begin{aligned}\boldsymbol{\sigma}_{pH}^{k} &= \hat{\boldsymbol{C}}_{pp}^{k}\boldsymbol{D}_{p}(F_{\tau}^{ik}N_{i}\boldsymbol{I})\boldsymbol{u}_{\tau i}^{k} + \hat{\boldsymbol{C}}_{pn}^{k}(F_{\tau}^{ik}N_{i}\boldsymbol{I})\boldsymbol{\sigma}_{n\tau i}^{k} \\ \boldsymbol{\epsilon}_{nH}^{k} &= \hat{\boldsymbol{C}}_{np}^{k}\boldsymbol{D}_{p}(F_{\tau}^{ik}N_{i}\boldsymbol{I})\boldsymbol{u}_{\tau i}^{k} + \hat{\boldsymbol{C}}_{nn}^{k}(F_{\tau}^{ik}N_{i}\boldsymbol{I})\boldsymbol{\sigma}_{n\tau i}^{k}\end{aligned} \tag{29}$$

Lastly, once all substitutions of the field variables and their variations just given by Eqs. (26)–(29) are introduced in RMVT, as stated in Eq. (10), for each k-layer of a representative finite element, gives rise to the following expression, in compact form:

$$\begin{aligned}\int_{\Omega}\int_{h^k}\big[\,&\delta\boldsymbol{u}_{sj}^{k\intercal}\boldsymbol{D}_{p}^{\intercal}(F_{s}^{jk}N_{j}\boldsymbol{I})\hat{\boldsymbol{C}}_{pp}^{k}\boldsymbol{D}_{p}(F_{\tau}^{ik}N_{i}\boldsymbol{I})\boldsymbol{u}_{\tau i}^{k} \\ &+ \delta\boldsymbol{u}_{sj}^{k\intercal}\boldsymbol{D}_{p}^{\intercal}(F_{s}^{jk}N_{j}\boldsymbol{I})\hat{\boldsymbol{C}}_{pn}^{k}(F_{\tau}^{ik}N_{i}\boldsymbol{I})\boldsymbol{\sigma}_{n\tau i}^{k} \\ &+ \delta\boldsymbol{u}_{sj}^{k\intercal}\boldsymbol{D}_{np}^{\intercal}(F_{s}^{jk}N_{j}\boldsymbol{I})(F_{\tau}^{ik}N_{i}\boldsymbol{I})\boldsymbol{\sigma}_{n\tau i}^{k} \\ &+ \delta\boldsymbol{u}_{sj}^{k\intercal}\boldsymbol{D}_{nz}^{\intercal}(F_{s}^{jk}N_{j}\boldsymbol{I})(F_{\tau}^{ik}N_{i}\boldsymbol{I})\boldsymbol{\sigma}_{n\tau i}^{k} \\ &+ \delta\boldsymbol{\sigma}_{nsj}^{k\intercal}(F_{s}^{jk}N_{j}\boldsymbol{I})\boldsymbol{D}_{np}(F_{\tau}^{ik}N_{i}\boldsymbol{I})\boldsymbol{u}_{\tau i}^{k} \\ &+ \delta\boldsymbol{\sigma}_{nsj}^{k\intercal}(F_{s}^{jk}N_{j}\boldsymbol{I})\boldsymbol{D}_{nz}(F_{\tau}^{ik}N_{i}\boldsymbol{I})\boldsymbol{u}_{\tau i}^{k} \\ &- \delta\boldsymbol{\sigma}_{nsj}^{k\intercal}(F_{s}^{jk}N_{j}\boldsymbol{I})\hat{\boldsymbol{C}}_{np}^{k}\boldsymbol{D}_{p}(F_{\tau}^{ik}N_{i}\boldsymbol{I})\boldsymbol{u}_{\tau i}^{k} \\ &- \delta\boldsymbol{\sigma}_{nsj}^{k\intercal}(F_{s}^{jk}N_{j}\boldsymbol{I})\hat{\boldsymbol{C}}_{nn}^{k}(F_{\tau}^{ik}N_{i}\boldsymbol{I})\boldsymbol{\sigma}_{n\tau i}^{k}\big]\,\mathrm{d}h^{k}\mathrm{d}\Omega = \delta L_{ext}^{k}\end{aligned} \tag{30}$$

where Ω denotes the in-plane finite element domain and h^k the thickness domain of each k-layer.

This expression can still be conveniently rearranged by grouping each vector field variable and its variation, and thus identifying the matrices arising, as follows:

$$\begin{aligned}&\delta\boldsymbol{u}_{sj}^{k\intercal}\big[\,\boldsymbol{K}_{uu}^{ks\tau ji}\boldsymbol{u}_{\tau i}^{k} + \boldsymbol{K}_{u\sigma}^{ks\tau ji}\boldsymbol{\sigma}_{n\tau i}^{k}\big] \\ &\quad+ \delta\boldsymbol{\sigma}_{nsj}^{k\intercal}\big[\,\boldsymbol{K}_{\sigma u}^{ks\tau ji}\boldsymbol{u}_{\tau i}^{k} + \boldsymbol{K}_{\sigma\sigma}^{ks\tau ji}\boldsymbol{\sigma}_{n\tau i}^{k}\big] = \delta L_{ext}^{k}\end{aligned} \tag{31}$$

where each matrix of size 3×3, namely, $\boldsymbol{K}_{uu}^{ks\tau ji}$, $\boldsymbol{K}_{u\sigma}^{ks\tau ji}$, $\boldsymbol{K}_{\sigma u}^{ks\tau ji}$ and $\boldsymbol{K}_{\sigma\sigma}^{ks\tau ji}$, is the so-called *Fundamental Nuclei* (FN) of the finite element stiffness matrix in the framework of CUF.

Most noteworthy, the major benefit of CUF to develop finite element models is that the expressions of all *Fundamental Nucleus* (FNs) are independent of the adopted thickness functions, and therefore, hold exactly the same for any degree of kinematic refinement desired. In detail, the explicit expressions of each FN, in both compact and expanded forms, of the proposed RMVT-based LW plate elements with NDK are here presented in Appendix A, for completeness.

Additionally, the layer external virtual work, as first stated in Eq. (9), can also follow the usual procedure to derive a consistent load vector. Considering that any imposed surface load acting on the k-layer is applied on a plane parallel to the plate mid-plane, the layer external virtual work can be expressed rather analogously, for a representative finite element (i.e. involving an integration in Ω as well), as shown:

$$\delta L_{ext}^{k} = \delta\boldsymbol{u}_{sj}^{k\intercal}\boldsymbol{P}_{u}^{ksj} \tag{32}$$

where the vector $\boldsymbol{P}_{u}^{ksj}$ of size 3×1 stands for the FN of the finite element load vector, which is variationally equivalent to the applied surface load, and can also accommodate external point loads accordingly, in such a case.

In the end, combining Eqs. (31)–(32), the following equations of the proposed RMVT-based LW plate elements with NDK can be established, for each k-layer, in compact form:

$$\begin{aligned}\delta\boldsymbol{u}_{sj}^{k\intercal}:&\quad \boldsymbol{K}_{uu}^{ks\tau ji}\boldsymbol{u}_{\tau i}^{k} + \boldsymbol{K}_{u\sigma}^{ks\tau ji}\boldsymbol{\sigma}_{n\tau i}^{k} = \boldsymbol{P}_{u}^{ksj} \\ \delta\boldsymbol{\sigma}_{nsj}^{k\intercal}:&\quad \boldsymbol{K}_{\sigma u}^{ks\tau ji}\boldsymbol{u}_{\tau i}^{k} + \boldsymbol{K}_{\sigma\sigma}^{ks\tau ji}\boldsymbol{\sigma}_{n\tau i}^{k} = 0\end{aligned} \tag{33}$$

Note that the FNs represent core units of the multilayered plate finite element stiffness matrix and load vector, which are then derived, as a whole, by looping on the indices involved throughout the assemblage process on the element level. In fact, the novel approach introduced by NDK is based on a suitable looping sequence, i.e.: loop on (j,i) associated with the j-local and i-local kinematics; loop on each k-layer; and loop on (s,τ), each dependent on the j-local and i-local

kinematics, respectively. Furthermore, when the j-local and i-local kinematics involved are different, sub-matrices on the layer and multilayer levels appear rectangular, rather than square. However, on the element level, all rectangular sub-matrices exist in pairs with their transpose, thus the finite element stiffness matrix remains square, regardless of the j, i-local kinematics involved in the element itself. Actually, the assemblage process of the finite element stiffness matrix is depicted in Fig. 4, when different j, i-local kinematics are involved, to make this clear. Besides, the finite element load vector follows the assemblage process on the element level analogously, and thus remains compatible with finite element stiffness matrix.

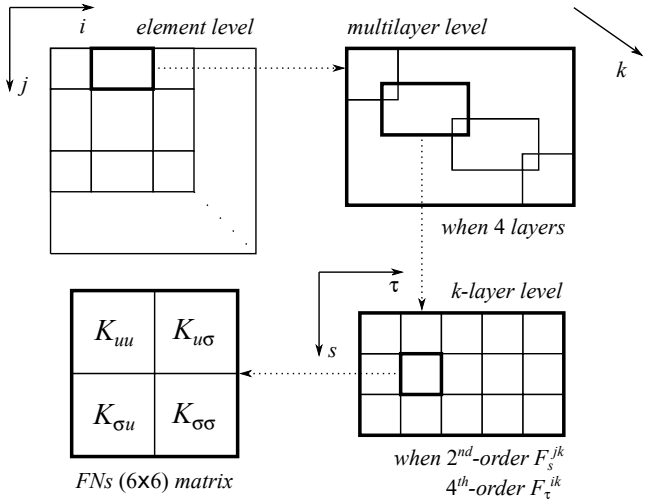

Figure 4: Assemblage process of the RMVT-based LW finite element stiffness matrix with NDK.

Another crucial feature to underline is that full integration by Gauss–Legendre quadrature is used in the numerical evaluation of the integral expressions of all FNs of the proposed RMVT-based LW plate elements with NDK and HLE combined. In other words, reduced or selective integration techniques commonly used to avoid shear-locking seem to be, in fact, unnecessary, as a direct result and a further benefit of using high p-order HLE as 2D shape functions.

7. Numerical results

The predictive capabilities of the proposed RMVT-based LW plate elements with NDK, involving high p-order (1D) Legendre thickness functions, to incorporate any degree of kinematic refinement as desired using CUF, combined with high p-order (2D) hierarchical Legendre expansions (HLE), are now demonstrated through a set of numerical results. The focus is on stress analysis of various multilayered composite plates, with different side-to-thickness ratios, under distinct loading conditions, considering well-known benchmark 3D exact solutions for assessment. In fact, for each benchmark, a series of global–local approaches are investigated and thoroughly assessed on both numerical accuracy and computational efficiency. In detail, three main benchmarks are studied, as follows:

- *Benchmark 1: composite laminates in cylindrical bending.*
  Based on the 3D exact solutions derived by Pagano et al. [41], two composite laminates are considered, namely, $(0°/90°/0°)$ and $(0°/90°)_2$, with $a/h = 4$, both in cylindrical bending by a sinusoidal load on the plate top surface along its x-axis, and simply supported on the plate edges $x = 0, a$. The 3D exact solutions are thus independent of the y-direction, which can be simulated by suitable boundary conditions on the plate edges $y = 0, b$, as described hereafter. In practice, the plate dimensions $a/b = 4$ are used for both composite laminates.
- *Benchmark 2: composite laminates under a bi-sinusoidal load.*
  Based on the 3D exact solutions derived by Pagano et al. [42], three square composite laminates $(0°/90°/0°)$ are considered, with $a/h = 4$, 10 and 100, in each case, under a bi-sinusoidal load on the plate top surface, and simply supported on all plate edges.
- *Benchmark 3: composite laminates under a localized uniform load.*
  Based on the 3D exact solutions provided by Biscani et al. [34], two square composite laminates are considered, namely, $(0°/90°/0°)$ and $(0°/90°)_2$, with $a/h = 10$, under a localized uniform load, applied on a square region of side $a/5$ centred on the plate top surface, and simply supported on all plate edges. In practice, the plate dimensions $a = b = 0.1$ m and the load $p_0 = 1$ MPa are used for both composite laminates.

The material properties of the unidirectional fibre reinforced composite layers used in each benchmark are summarized in Table 1, in line with the original works by Pagano [41, 42] and Biscani et al. [34]. To be clear, the subscripts L, T and Z are relative to the layer material coordinate system, to denote the fibre longitudinal direction, its transverse direction in-plane and out-of-plate, respectively.

Table 1: Material properties of the composite layers used in each benchmark (BM).

Property	E_L[GPa]	$E_T = E_Z$[GPa]	$\nu_{LT} = \nu_{LZ}$[–]	ν_{TZ}[–]	$G_{LT} = G_{LZ}$[GPa]	G_{TZ}[GPa]
BM 1&2 [41, 42]	$25E_T$	$7^{\dagger}$	0.25	0.25	$0.5E_T$	$0.2E_T$
BM 3 [34]	132.5	10.8	0.24	0.49	5.7	3.4

† Reference to scale nondimensionalized results: $E_T = 7\,\text{GPa}\,(\approx 10^6\,\text{psi})$ is used in practice, in line with Pagano [41, 42].

Moreover, in agreement with the 3D exact solutions derived by Pagano [41, 42], the results regarding the benchmarks 1 and 2 are presented in a nondimensionalized form, as follows:

$$\begin{aligned}
&[\bar{u}, \bar{v}] = \frac{E_T h^2}{p_0 a^3}\,[u, v]\,, \quad \bar{w} = \frac{100 E_T h^3}{p_0 a^4} w \\
&[\bar{\sigma}_{xz}, \bar{\sigma}_{yz}] = \frac{h}{p_0 a}\,[\sigma_{xz}, \sigma_{yz}]\,, \quad \bar{\sigma}_{zz} = \frac{\sigma_{zz}}{p_0} \\
&[\bar{\sigma}_{xx}, \bar{\sigma}_{yy}, \bar{\sigma}_{xy}] = \frac{h^2}{p_0 a^2}\,[\sigma_{xx}, \sigma_{yy}, \sigma_{xy}]
\end{aligned} \tag{34}$$

where p_0 stands for the intensity of the load and E_T is set by the layers material properties, which are all together used as reference scale factors, along with the plate dimensions, a and h.

Also noteworthy is the fact that not all the 3D exact solutions here presented for assessment, regarding the benchmarks 1 and 2, are actually provided in the original works by Pagano [41, 42]. In reality, a number of 3D exact solutions are here first-ever made available, as derived from a more recent work by Moleiro et al. [43] focused on benchmark 3D exact solutions for piezoelectric multilayered composite plates according to Pagano's solution method. In particular, all the 3D exact solutions regarding the benchmarks 1 and 2, originally introduced by Pagano [41, 42], can therefore be reproduced and presented herein with as much precision as desired.

7.1. Benchmark 1: composite laminates in cylindrical bending

Considering the stress analysis of the composite laminates $(0°/90°/0°)$ and $(0°/90°)_2$, with $a/h = 4$, in cylindrical bending, the following load and boundary conditions are used in practice, with $a/b = 4$ as well:

Sinusoidal load

$$p(x) = p_0 \sin\left(\tfrac{\pi x}{a}\right) \tag{35}$$

Boundary conditions

$$\begin{aligned}
&\text{At } x = 0, a: \quad v = w = 0; \quad u\left(0, 0, -\tfrac{h}{2}\right) = 0 \\
&\text{At } y = 0, b: \quad v = 0 \\
&\text{At } z = -\tfrac{h}{2}: \quad \sigma_{zz} = \sigma_{xz} = \sigma_{yz} = 0 \\
&\text{At } z = \tfrac{h}{2}: \quad \sigma_{xz} = \sigma_{yz} = 0
\end{aligned} \tag{36}$$

In detail, besides simply supported conditions on the plate edges $x = 0, a$, symmetry conditions on the plate edges $y = 0, b$ are employed, in line with the 3D exact solutions that are independent of the y-direction. Moreover, to prevent rigid body motion along the x-axis, one point of zero u-displacement is included. Most notably, as a benefit of RMVT-based elements, the real traction free boundary conditions on the plate top and bottom surfaces can also be accurately imposed.

As a preliminary step, a convergence study of RMVT-based LW plate elements in the mesh is performed, without the use of NDK, simply by standard approaches of finite element refinement, i.e.: h-refinement by increasing the number of elements in the mesh, and p-refinement by increasing the (high) p-order of the HLE, denoted as HLEp. The results of this convergence study are shown in Table 2, which is focused on HLE4 and HLE5. In fact, as demonstrated also by Zappino et al. [40], the accuracy improvement by increasing the p-order of the HLE is most efficient computationally when HLE4

or HLE5 are considered. Still, in this preliminary step, the kinematic assumptions hold equally for all RMVT-based LW plate elements throughout the mesh, in line with such standard refinement approaches. Considering that $a/h = 4$ is typical of thick laminates, a high degree of kinematic refinement is most suitable. Hence, in this convergence study, the kinematics adopted for the composite laminates $(0°/90°/0°)$ and $(0°/90°)_2$ involve for each case, either 3 layers or 4 layers, with each layer using 4^{th}-order Legendre thickness functions, denoted as 3L4 or 4L4, respectively.

Table 2: Composite laminates $(0°/90°/0°)$ and $(0°/90°)_2$ in cylindrical bending $(a/h = 4)$: convergence study by standard h-refinement and p-refinement of RMVT-based LW plate elements in the mesh (without the use of NDK).

$(0°/90°/0°)$					$(0°/90°)_2$				
Mesh ⊥ Kinematics	$\bar{w}$ $(\frac{a}{2}, \frac{b}{2}, 0)$	$\bar{\sigma}_{xx}$ $(\frac{a}{2}, \frac{b}{2}, \frac{h}{2})$	$\bar{\sigma}_{zz}$ $(\frac{a}{2}, \frac{b}{2}, 0)$	DOFs	Mesh ⊥ Kinematics	$\bar{w}$ $(\frac{a}{2}, \frac{b}{2}, 0)$	$\bar{\sigma}_{xx}$ $(\frac{a}{2}, \frac{b}{2}, -\frac{h}{2})$	$\bar{\sigma}_{zz}$ $(\frac{a}{2}, \frac{b}{2}, 0)$	DOFs
3D [41, 43]	2.8872	1.1755	0.4988		3D [41, 43]	4.1801	−1.5593	0.6530	
5×1 HLE4 ⊥ 3L4$^{\triangleright}$	2.8872	1.1743	0.4988	$^{\triangleright}$5070	5×1 HLE4 ⊥ 4L4$^{\triangleright}$	4.1801	−1.5587	0.6534	$^{\triangleright}$6630
4×1 HLE4 ⊥ 3L4	2.8872	1.1741	0.4989	4134	4×1 HLE4 ⊥ 4L4	4.1800	−1.5585	0.6531	5406
3×1 HLE4 ⊥ 3L4	2.8871	1.1740	0.4989	3198	3×1 HLE4 ⊥ 4L4	4.2079	−1.5905	0.5437	4182
2×1 HLE4 ⊥ 3L4	2.8860	1.1712	0.4987	2262	2×1 HLE4 ⊥ 4L4	4.1741	−1.6169	0.6440	2958
5×1 HLE5 ⊥ 3L4	2.8872	1.1743	0.4989	7098	5×1 HLE5 ⊥ 4L4	4.1801	−1.5588	0.6531	9282
4×1 HLE5 ⊥ 3L4$^{\triangleright}$	2.8872	1.1743	0.4989	$^{\triangleright}$5772	4×1 HLE5 ⊥ 4L4$^{\triangleright}$	4.1801	−1.5588	0.6531	$^{\triangleright}$7548
3×1 HLE5 ⊥ 3L4	2.8872	1.1743	0.4989	4446	3×1 HLE5 ⊥ 4L4	4.1767	−1.5860	0.6680	5814

$^{\triangleright}$ Selection of meshes using HLE4 or HLE5 to ensure fully converged results, regardless of the lamination scheme.

As demonstrated by Table 2, the selection of the most suitable meshes to ensure fully converged results, under equal kinematic assumptions, regardless of the lamination scheme, seems to rest on a mesh 5×1 HLE4 or a mesh 4×1 HLE5. However, considering that between the two meshes, the number of degrees of freedom (DOFs) involved with HLE5 are somewhat higher, the computational efficiency provided by HLE4 shows the most potential.

Subsequently, the global–local stress analysis of the composite laminates $(0°/90°/0°)$ and $(0°/90°)_2$, with $a/h = 4$, in cylindrical bending, by RMVT-based LW plate elements with NDK, is pre-established on a mesh 5×1 using HLE4 or, in alternative, HLE5. Specifically, the global–local regions in this mesh 5×1 with different degrees of kinematic refinement assigned locally to the desired nodes of RMVT-based LW plate elements are depicted in Fig. 5, for clearness. In essence, three different global–local approaches can be considered based on the corresponding global–local regions, namely, GLa, GLb or GLc, with a higher-degree of kinematic refinement towards the centre of the laminate, in line with the higher intensity of the sinusoidal load. In addition, note that these global–local approaches purposely do not take advantage of the problem symmetry, which would obviously be even more efficient computationally, to demonstrate more precisely the NDK capabilities throughout the mesh, including gradual effects in transition zones.

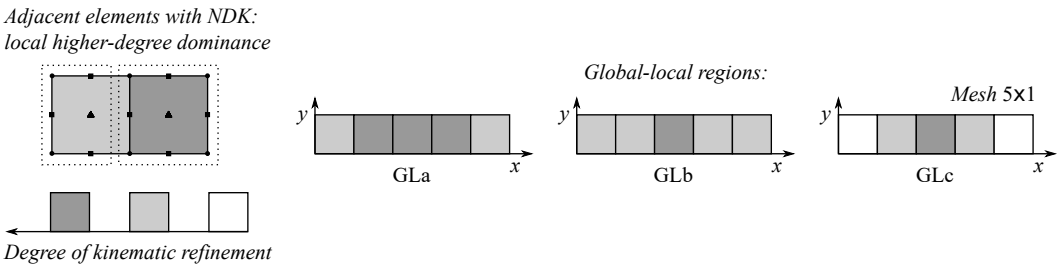

Figure 5: Global-local regions of RMVT-based LW plate elements with NDK, namely, GLa, GLb or GLc, as considered in the mesh for a global–local analysis of the composite laminates $(0°/90°/0°)$ and $(0°/90°)_2$ in cylindrical bending $(a/h = 4)$.

The results of the intended stress analysis of the composite laminates $(0°/90°/0°)$ and $(0°/90°)_2$, with $a/h = 4$, in cylindrical bending, by RMVT-based LW plate elements, with or without the use of NDK for a global–local analysis, are summarized in Table 3 and Table 4, respectively.

To be clear, the reasoning of the kinematic designations is the following: when the kinematic assumptions hold equally throughout the mesh, the designation N_lLp is used, meaning N_l layers, with each layer using p-order Legendre thickness functions; when a global–local approach is considered, with different degrees of kinematic refinement throughout the mesh corresponding to the global–local regions GLa, GLb or GLc, the designations N_lLp-p,GLa, N_lLp-p,GLb or N_lLp-p-p,GLc are used respectively, where the p-sequence indicates in ascending order the layers p-order Legendre thickness functions involved in the distinct zones of refinement in the mesh.

A close examination of Tables 3–4 shows that compared to the most computationally demanding standard approach, under equal kinematic assumptions, with each layer using 4^{th}-order Legendre thickness functions, namely, 3L4 or 4L4

Table 3: Composite laminate $(0°/90°/0°)$ in cylindrical bending $(a/h = 4)$: displacements and stresses by RMVT-based LW plate elements with or without the use of NDK for a global–local analysis.

Mesh ⊥ Kinematics	$\bar{w}$ $(\frac{a}{2}, \frac{b}{2}, 0)$	$\bar{\sigma}_{xx}$ $(\frac{a}{2}, \frac{b}{2}, -\frac{h}{2})$	$\bar{\sigma}_{xx}{}^{\dagger}$ $(\frac{a}{2}, \frac{b}{2}, -\frac{h}{6})$	$\bar{\sigma}_{xx}$ $(\frac{a}{2}, \frac{b}{2}, 0)$	$\bar{\sigma}_{xx}{}^{\dagger}$ $(\frac{a}{2}, \frac{b}{2}, \frac{h}{6})$	$\bar{\sigma}_{xx}$ $(\frac{a}{2}, \frac{b}{2}, \frac{h}{2})$	$\bar{\sigma}_{xz}$ $(0, \frac{b}{2}, 0)$	$\bar{\sigma}_{zz}$ $(\frac{a}{2}, \frac{b}{2}, 0)$	DOFs
3D [41, 43]	2.8872	−1.1315	0.2536	0.0061	−0.2977	1.1755	0.3579	0.4988	
5×1 HLE4 ⊥ 3L4	2.8872	−1.1305	0.2536	0.0061	−0.2978	1.1743	0.3578	0.4988	5070
5×1 HLE4 ⊥ 3L3-4,GLa	2.8872	−1.1305	0.2536	0.0061	−0.2977	1.1743	0.3580	0.4987	4638
5×1 HLE4 ⊥ 3L3-4,GLb$^{\triangleright}$	2.8870	−1.1302	0.2552	0.0061	−0.2994	1.1743	0.3580	0.4977	$^{\triangleright}$4206
5×1 HLE4 ⊥ 3L3	2.8877	−1.0929	0.2181	0.0060	−0.2628	1.1358	0.3579	0.4988	3900
5×1 HLE4 ⊥ 3L2-3-4,GLc	2.8865	−1.1301	0.2567	0.0061	−0.3009	1.1745	0.3498	0.4973	3774
5×1 HLE4 ⊥ 3L2	2.8931	−1.0508	0.2607	0.0065	−0.3069	1.0778	0.3634	0.5106	2730
5×1 HLE5 ⊥ 3L4	2.8872	−1.1306	0.2536	0.0061	−0.2978	1.1743	0.3578	0.4989	7098
5×1 HLE5 ⊥ 3L3-4,GLa	2.8872	−1.1306	0.2537	0.0061	−0.2978	1.1743	0.3580	0.4990	6486
5×1 HLE5 ⊥ 3L3-4,GLb	2.8870	−1.1303	0.2553	0.0061	−0.2993	1.1743	0.3580	0.4983	5874
5×1 HLE5 ⊥ 3L3	2.8877	−1.0930	0.2181	0.0060	−0.2628	1.1358	0.3579	0.4988	5460
5×1 HLE5 ⊥ 3L2-3-4,GLc	2.8865	−1.1303	0.2567	0.0061	−0.3008	1.1744	0.3499	0.4981	5262

† Maximum value of interlaminar discontinuity exhibited by the composite layer of 0°.
$^{\triangleright}$ Selection of GL approach using NDK for optimal high numerical accuracy and computational efficiency.

Table 4: Composite laminate $(0°/90°)_2$ in cylindrical bending $(a/h = 4)$: displacements and stresses by RMVT-based LW plate elements with or without the use of NDK for a global–local analysis.

Mesh ⊥ Kinematics	$\bar{w}$ $(\frac{a}{2}, \frac{b}{2}, 0)$	$\bar{\sigma}_{xx}$ $(\frac{a}{2}, \frac{b}{2}, -\frac{h}{2})$	$\bar{\sigma}_{xx}{}^{\dagger}$ $(\frac{a}{2}, \frac{b}{2}, -\frac{h}{4})$	$\bar{\sigma}_{xx}{}^{\dagger}$ $(\frac{a}{2}, \frac{b}{2}, 0)$	$\bar{\sigma}_{xx}{}^{\dagger}$ $(\frac{a}{2}, \frac{b}{2}, \frac{h}{4})$	$\bar{\sigma}_{xx}$ $(\frac{a}{2}, \frac{b}{2}, \frac{h}{2})$	$\bar{\sigma}_{xz}$ $(0, \frac{b}{2}, 0)$	$\bar{\sigma}_{zz}$ $(\frac{a}{2}, \frac{b}{2}, 0)$	DOFs
3D [41, 43]	4.1801	−1.5593	0.1373	−0.2489	1.4022	0.1642	0.4805	0.6530	
5×1 HLE4 ⊥ 4L4	4.1801	−1.5587	0.1374	−0.2488	1.4018	0.1642	0.4804	0.6534	6630
5×1 HLE4 ⊥ 4L3-4,GLa	4.1801	−1.5587	0.1374	−0.2487	1.4018	0.1642	0.4807	0.6528	6054
5×1 HLE4 ⊥ 4L3-4,GLb$^{\triangleright}$	4.1799	−1.5593	0.1380	−0.2494	1.4022	0.1643	0.4806	0.6522	$^{\triangleright}$5478
5×1 HLE4 ⊥ 4L3	4.1803	−1.5335	0.1137	−0.2254	1.3768	0.1653	0.4805	0.6538	5070
5×1 HLE4 ⊥ 4L2-3-4,GLc	4.1797	−1.5597	0.1388	−0.2501	1.4026	0.1643	0.4915	0.6510	4902
5×1 HLE4 ⊥ 4L2	4.1824	−1.4973	0.1487	−0.2478	1.3523	0.1622	0.4718	0.6718	3510
5×1 HLE5 ⊥ 4L4	4.1801	−1.5588	0.1374	−0.2488	1.4019	0.1642	0.4804	0.6531	9282
5×1 HLE5 ⊥ 4L3-4,GLa	4.1801	−1.5588	0.1374	−0.2488	1.4019	0.1642	0.4806	0.6532	8466
5×1 HLE5 ⊥ 4L3-4,GLb	4.1800	−1.5594	0.1383	−0.2495	1.4025	0.1642	0.4806	0.6524	7650
5×1 HLE5 ⊥ 4L3	4.1803	−1.5335	0.1137	−0.2255	1.3768	0.1653	0.4805	0.6538	7098
5×1 HLE5 ⊥ 4L2-3-4,GLc	4.1797	−1.5599	0.1391	−0.2503	1.4029	0.1641	0.4916	0.6529	6834

† Maximum value of interlaminar discontinuity exhibited by the composite layer of 0°.
$^{\triangleright}$ Selection of GL approach using NDK for optimal high numerical accuracy and computational efficiency.

for each composite laminate, the global–local approaches can actually maintain a high level of numerical accuracy with a significant reduction of computational efforts, as shown by the number of DOFs involved. Specifically, the selection of the optimal global–local approach, which ensures exactly the same high level of numerical accuracy as the most demanding standard approach, thus no loss of numerical accuracy locally, while involving the lowest number of DOFs, seems to rest on the kinematics 3L3-4,GLb or 4L3-4,GLb for each composite laminate. In fact, this trend is demonstrated whether a mesh 5×1 HLE4 or a mesh 5×1 HLE5 is considered, although (as before) the computational efficiency provided by HLE4 seems to be preferable, since fewer DOFs are involved. Moreover, even the less demanding global–local approach, namely, the kinematics 3L2-3-4,GLc or 4L2-3-4,GLc for each composite laminate, is still able to achieve more accurate results than a fairly comparable standard approach, under equal kinematic assumptions, namely, 3L3 or 4L3, which actually involves slightly more computational efforts. Hence, the use of different degrees of kinematic refinement throughout the mesh is shown to be advantageous even if no reduction of computational efforts are made.

A more insightful description of the global–local stress analysis of the composite laminates $(0°/90°/0°)$ and $(0°/90°)_2$, with $a/h = 4$, in cylindrical bending, by RMVT-based LW plate elements using NDK throughout the mesh, is provided by Fig. 6, showing contour distributions of transverse stresses according to the optimal global–local approach, namely, 3L3-4,GLb or 4L3-4,GLb for each composite laminate, respectively.

As apparent from Fig. 6, as long as the different degrees of kinematic refinement are pre-established throughout the mesh in a gradual form, the overall solution of a global–local analysis by RMVT-based LW plate elements using NDK can preserve the quality of the numerical results in the transitional regions, besides the local and global regions. Thus, if employed properly, no abnormal (localized) side-effects seem to arise from the use of NDK capabilities.

Furthermore, to complete in greater detail the global–local stress analysis of the composite laminates $(0°/90°/0°)$ and $(0°/90°)_2$, with $a/h = 4$, in cylindrical bending, Fig. 7 shows the through-thickness distributions of both transverse and in-plane stresses by RMVT-based LW plate elements using NDK according to the same optimal global–local approach,

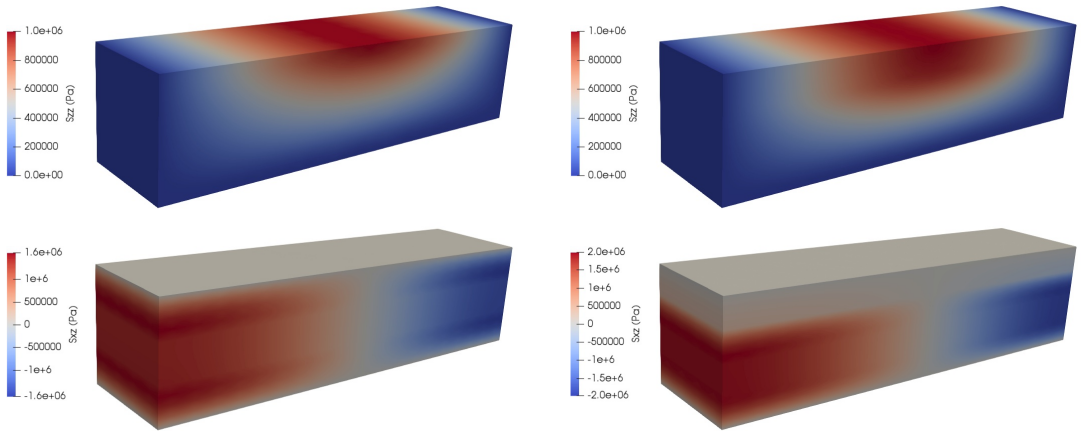

Figure 6: Composite laminates $(0°/90°/0°)$ and $(0°/90°)_2$ in cylindrical bending $(a/h = 4)$: transverse stresses distributions by RMVT-based LW plate elements using NDK for a global–local analysis, i.e. 3L3-4,GLb (on the left) and 4L3-4,GLb (on the right), respectively.

namely, 3L3-4,GLb or 4L3-4,GLb for each composite laminate, respectively. In fact, the through-thickness distributions predicted demonstrate a high level of numerical accuracy, in perfect agreement with the 3D exact solutions, even in the case of transverse stresses evaluated at a zone of lower degree of kinematic refinement in the mesh (as set by GLb).

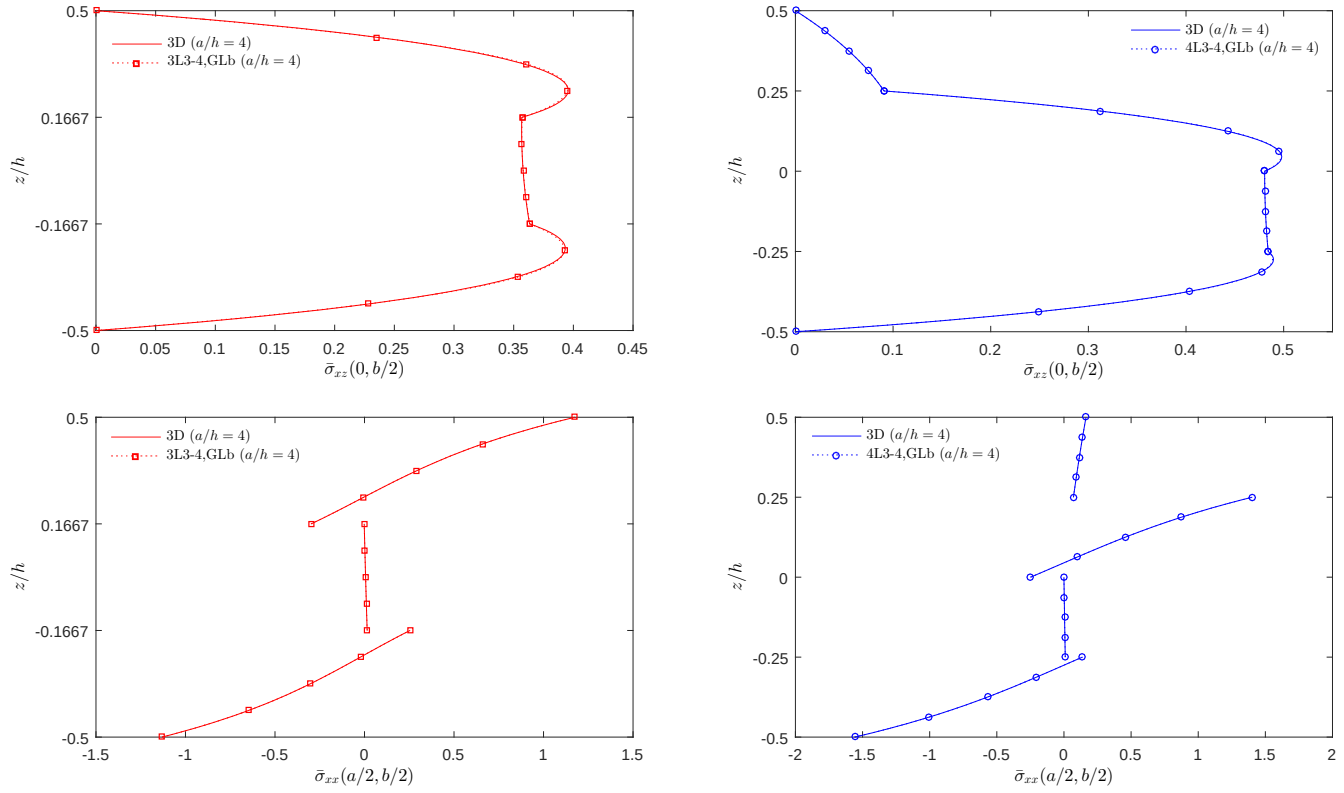

Figure 7: Composite laminates $(0°/90°/0°)$ and $(0°/90°)_2$ in cylindrical bending $(a/h = 4)$: through-thickness distributions by RMVT-based LW plate elements using NDK for a global–local analysis, alongside 3D exact solutions as derived from the work by Moleiro et al. [43].

7.2. Benchmark 2: composite laminates under a bi-sinusoidal load

For the stress analysis of the simply supported square composite laminates $(0°/90°/0°)$, with $a/h = 4$, 10 and 100, under a bi-sinusoidal load, the following load and boundary conditions are used in practice:

Bi-sinusoidal load

$$p(x,y) = p_0 \sin\left(\tfrac{\pi x}{a}\right) \sin\left(\tfrac{\pi y}{a}\right) \tag{37}$$

Boundary conditions

$$\begin{aligned} &\text{At } x = 0, a: \quad v = w = 0 \\ &\text{At } y = 0, b: \quad u = w = 0 \\ &\text{At } z = -\tfrac{h}{2}: \quad \sigma_{zz} = \sigma_{xz} = \sigma_{yz} = 0 \\ &\text{At } z = \tfrac{h}{2}: \quad \sigma_{xz} = \sigma_{yz} = 0 \end{aligned} \tag{38}$$

Specifically, besides the usual simply supported conditions on all plate edges, the real traction free boundary conditions on the plate top and bottom surfaces can also be accurately imposed, due to the added value of RMVT-based elements.

The intended global–local stress analysis of the square composite laminates (0°/90°/0°), with $a/h = 4$, 10 and 100, under a bi-sinusoidal load, by RMVT-based LW plate elements with NDK is now pre-established on a mesh 5×5 HLE4. This mesh ensures fully converged results, under equal kinematic assumptions, even in the case of thick laminates with $a/h = 4$, as long as a high degree of kinematic refinement is involved, as confirmed in a convergence study by standard h- and p-refinement approaches, omitted here for brevity, but also reasonably expected in view of the previous benchmark. Moreover, this mesh 5×5 using HLE4 is considered to begin with, in line with the promising computationally efficiency already shown by HLE4, even though HLE5 would also be a fair alternative.

Analogously to the previous benchmark, the global–local regions in this mesh 5×5 HLE4 with different degrees of kinematic refinement assigned locally to the desired nodes of RMVT-based LW plate elements are depicted in Fig. 8, for clearness. Hence, different global–local approaches can be considered based on the pre-established global–local regions, namely, GLa, GLb or GLc, with a higher-degree of kinematic refinement towards the centre of the laminate, in line with the higher intensity of the sinusoidal load. Actually, considering the range of side-to-thickness ratios from thick to thin laminates under analysis, the global–local regions GLa, GLb or GLc can each be employed for more than one global–local approach. For instance, the kinematics 3L3-4,GLa or 3L2-3,GLa both refer to the global–local regions GLa, but in the former each layer using 3^{rd}- or 4^{th}-order thickness functions throughout the mesh, and the last using 2^{nd}- or 3^{rd}-order thickness functions, instead, in the zones of lower or higher degree of kinematic refinement in the mesh, as set by GLa. Furthermore, much like the previous benchmark, these global–local approaches purposely do not take advantage of the problem symmetries, to demonstrate more precisely the NDK capabilities throughout the entire mesh, though a quarter model of the plate for this benchmark would obviously be even more efficient computationally.

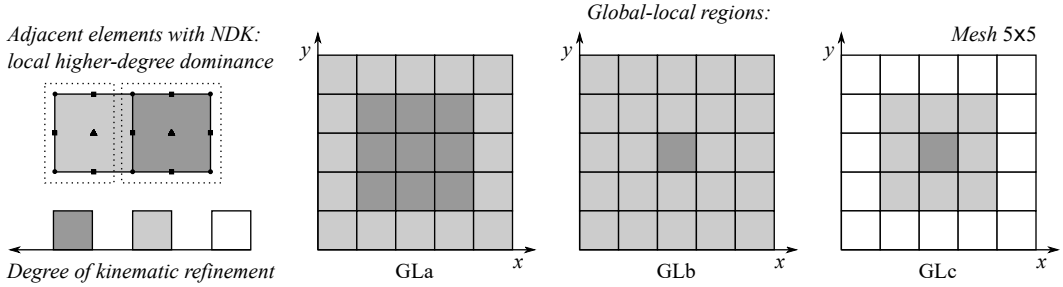

Figure 8: Global-local regions of RMVT-based LW plate elements with NDK, namely, GLa, GLb or GLc, as considered in the mesh for a global–local analysis of the composite laminates (0°/90°/0°) under a bi-sinusoidal load ($a/h = 4, 10, 100$).

The ensuing results of stress analysis of the square composite laminates (0°/90°/0°), with $a/h = 4$, 10 and 100, under a bi-sinusoidal load, by RMVT-based LW plate elements, with or without the use of NDK for a global–local analysis, are shown in Table 5, Table 6 and Table 7, respectively.

Examining Tables 5–7, each at a time, comparing with the most demanding standard approach, under equal kinematic assumptions (shown in the first line of results in each table as a baseline reference), the selection of the optimal global–local approach, which ensures exactly the same high level of numerical accuracy, while involving the lowest number of DOFs, can be easily identified going down each line, systematically in each table. Specifically, for the thick laminates with $a/h = 4$, the optimal global–local approach seems to rest on the kinematics 3L3-4,GLb, much like the previous benchmark also involving thick laminates. However, as the side-to-thickness ratios increases towards thinner laminates, the degree of kinematic refinement can be less demanding computationally, as the through-thickness distributions of both displacements and stresses become closer to piecewise linear distributions. In fact, for the moderately thick laminates

Table 5: Composite laminate (0°/90°/0°) under a bi-sinusoidal load ($a/h = 4$): displacements and stresses by RMVT-based LW plate elements with or without the use of NDK for a global–local analysis.

Mesh ⊥ Kinematics	$\bar{w}$ $(\frac{a}{2}, \frac{a}{2}, 0)$	$\bar{\sigma}_{xx}$ $(\frac{a}{2}, \frac{a}{2}, -\frac{h}{2})$	$\bar{\sigma}_{xx}$ $(\frac{a}{2}, \frac{a}{2}, \frac{h}{2})$	$\bar{\sigma}_{yy}{}^{\dagger}$ $(\frac{a}{2}, \frac{a}{2}, -\frac{h}{6})$	$\bar{\sigma}_{yy}{}^{\dagger}$ $(\frac{a}{2}, \frac{a}{2}, \frac{h}{6})$	$\bar{\sigma}_{xy}$ $(0, 0, -\frac{a}{2})$	$\bar{\sigma}_{xy}$ $(0, 0, \frac{a}{2})$	$\bar{\sigma}_{xz}$ $(0, \frac{a}{2}, 0)$	$\bar{\sigma}_{yz}$ $(\frac{a}{2}, 0, 0)$	$\bar{\sigma}_{zz}$ $(\frac{a}{2}, \frac{a}{2}, 0)$	DOFs
3D [42, 43]	2.0059	−0.7548	0.8008	−0.5563	0.5341	0.0505	−0.0511	0.2559	0.2172	0.4927	
5×5 HLE4 ⊥ 3L4	2.0058	−0.7539	0.7997	−0.5557	0.5335	0.0504	−0.0510	0.2559	0.2172	0.4928	18798
5×5 HLE4 ⊥ 3L3-4,GLa	2.0058	−0.7538	0.7997	−0.5557	0.5335	0.0504	−0.0510	0.2560	0.2186	0.4926	16206
5×5 HLE4 ⊥ 3L3-4,GLb$^{\triangleright}$	2.0055	−0.7538	0.8002	−0.5560	0.5339	0.0504	−0.0509	0.2560	0.2189	0.4913	$^{\triangleright}$14766
5×5 HLE4 ⊥ 3L3	2.0063	−0.7267	0.7716	−0.5297	0.5082	0.0504	−0.0510	0.2560	0.2189	0.4926	14460
5×5 HLE4 ⊥ 3L2-3-4,GLc	2.0051	−0.7537	0.8004	−0.5566	0.5345	0.0491	−0.0495	0.2496	0.2169	0.4911	12174
5×5 HLE4 ⊥ 3L2-3,GLa	2.0062	−0.7268	0.7719	−0.5298	0.5080	0.0491	−0.0495	0.2496	0.2170	0.4929	11868
5×5 HLE4 ⊥ 3L2-3,GLb	2.0066	−0.7241	0.7690	−0.5305	0.5080	0.0485	−0.0487	0.2580	0.2192	0.4950	10428
5×5 HLE4 ⊥ 3L2	2.0078	−0.7003	0.7337	−0.5303	0.5023	0.0485	−0.0487	0.2595	0.2194	0.4776	10122

† Maximum value of interlaminar discontinuity exhibited by the composite layer of 90°.
$^{\triangleright}$ Selection of GL approach using NDK for optimal high numerical accuracy and computational efficiency.

Table 6: Composite laminate (0°/90°/0°) under a bi-sinusoidal load ($a/h = 10$): displacements and stresses by RMVT-based LW plate elements with or without the use of NDK for a global–local analysis.

Mesh ⊥ Kinematics	$\bar{w}$ $(\frac{a}{2}, \frac{a}{2}, 0)$	$\bar{\sigma}_{xx}$ $(\frac{a}{2}, \frac{a}{2}, -\frac{h}{2})$	$\bar{\sigma}_{xx}$ $(\frac{a}{2}, \frac{a}{2}, \frac{h}{2})$	$\bar{\sigma}_{yy}{}^{\dagger}$ $(\frac{a}{2}, \frac{a}{2}, -\frac{h}{6})$	$\bar{\sigma}_{yy}{}^{\dagger}$ $(\frac{a}{2}, \frac{a}{2}, \frac{h}{6})$	$\bar{\sigma}_{xy}$ $(0, 0, -\frac{a}{2})$	$\bar{\sigma}_{xy}$ $(0, 0, \frac{a}{2})$	$\bar{\sigma}_{xz}$ $(0, \frac{a}{2}, 0)$	$\bar{\sigma}_{yz}$ $(\frac{a}{2}, 0, 0)$	$\bar{\sigma}_{zz}$ $(\frac{a}{2}, \frac{a}{2}, 0)$	DOFs
3D [42, 43]	0.7530	−0.5898	0.5906	−0.2882	0.2845	0.0290	−0.0288	0.3573	0.1228	0.4994	
5×5 HLE4 ⊥ 3L4	0.7530	−0.5894	0.5903	−0.2882	0.2845	0.0290	−0.0288	0.3573	0.1156	0.4967	18798
5×5 HLE4 ⊥ 3L3-4,GLa	0.7530	−0.5896	0.5904	−0.2881	0.2844	0.0289	−0.0288	0.3573	0.1229	0.4994	16206
5×5 HLE4 ⊥ 3L3-4,GLb	0.7530	−0.5896	0.5904	−0.2880	0.2843	0.0289	−0.0288	0.3573	0.1230	0.4991	14766
5×5 HLE4 ⊥ 3L3	0.7530	−0.5873	0.5880	−0.2858	0.2821	0.0289	−0.0288	0.3573	0.1230	0.4994	14460
5×5 HLE4 ⊥ 3L2-3-4,GLc$^{\triangleright}$	0.7530	−0.5896	0.5904	−0.2880	0.2843	0.0288	−0.0286	0.3550	0.1226	0.4989	$^{\triangleright}$12174
5×5 HLE4 ⊥ 3L2-3,GLa	0.7530	−0.5873	0.5880	−0.2858	0.2820	0.0288	−0.0286	0.3550	0.1226	0.4995	11868
5×5 HLE4 ⊥ 3L2-3,GLb	0.7530	−0.5875	0.5883	−0.2857	0.2819	0.0288	−0.0286	0.3586	0.1230	0.5004	10428
5×5 HLE4 ⊥ 3L2	0.7530	−0.5846	0.5849	−0.2856	0.2815	0.0288	−0.0286	0.3586	0.1230	0.4911	10122

† Maximum value of interlaminar discontinuity exhibited by the composite layer of 90°.
$^{\triangleright}$ Selection of GL approach using NDK for optimal high numerical accuracy and computational efficiency.

Table 7: Composite laminate (0°/90°/0°) under a bi-sinusoidal load ($a/h = 100$): displacements and stresses by RMVT-based LW plate elements with or without the use of NDK for a global–local analysis.

Mesh ⊥ Kinematics	$\bar{w}$ $(\frac{a}{2}, \frac{a}{2}, 0)$	$\bar{\sigma}_{xx}$ $(\frac{a}{2}, \frac{a}{2}, -\frac{h}{2})$	$\bar{\sigma}_{xx}$ $(\frac{a}{2}, \frac{a}{2}, \frac{h}{2})$	$\bar{\sigma}_{yy}{}^{\dagger}$ $(\frac{a}{2}, \frac{a}{2}, -\frac{h}{6})$	$\bar{\sigma}_{yy}{}^{\dagger}$ $(\frac{a}{2}, \frac{a}{2}, \frac{h}{6})$	$\bar{\sigma}_{xy}$ $(0, 0, -\frac{a}{2})$	$\bar{\sigma}_{xy}$ $(0, 0, \frac{a}{2})$	$\bar{\sigma}_{xz}$ $(0, \frac{a}{2}, 0)$	$\bar{\sigma}_{yz}$ $(\frac{a}{2}, 0, 0)$	$\bar{\sigma}_{zz}$ $(\frac{a}{2}, \frac{a}{2}, 0)$	DOFs
3D [42, 43]	0.4347	−0.5393	0.5393	−0.1808	0.1808	0.0214	−0.0214	0.3947	0.0828	0.5000	
5×5 HLE4 ⊥ 3L3	0.4347	−0.5391	0.5391	−0.1808	0.1807	0.0214	−0.0214	0.3953	0.0829	0.5000	14460
5×5 HLE4 ⊥ 3L2-3-4,GLc	0.4347	−0.5391	0.5391	−0.1808	0.1807	0.0214	−0.0214	0.3952	0.0829	0.5000	12174
5×5 HLE4 ⊥ 3L2-3,GLa	0.4347	−0.5391	0.5391	−0.1808	0.1807	0.0214	−0.0214	0.3952	0.0829	0.5000	11868
5×5 HLE4 ⊥ 3L2-3,GLb$^{\triangleright}$	0.4347	−0.5391	0.5391	−0.1808	0.1807	0.0214	−0.0214	0.3953	0.0829	0.5006	$^{\triangleright}$10428
5×5 HLE4 ⊥ 3L2	0.4347	−0.5391	0.5391	−0.1808	0.1807	0.0214	−0.0214	0.3953	0.0829	0.4944	10122
5×5 HLE4 ⊥ 3L1-2-3,GLc	0.4347	−0.5387	0.5387	−0.1803	0.1803	0.0218	−0.0218	0.4255	0.0523	0.5058	7836
5×5 HLE4 ⊥ 3L1	0.4772	−0.4001	0.3994	−0.0362	0.0368	0.0229	−0.0228	0.4336	0.0448	0.5909	5784

† Maximum value of interlaminar discontinuity exhibited by the composite layer of 90°.
$^{\triangleright}$ Selection of GL approach using NDK for optimal high numerical accuracy and computational efficiency.

with $a/h = 10$, the optimal global–local approach seems to rest on the kinematics 3L2-3-4,GLc, which still ensures a high numerical accuracy, including for the in-plane stresses when compared to the kinematics that follow with slightly less DOFs. Moreover, for the thin laminates with $a/h = 100$, the optimal global–local approach seems to rest on an even less demanding kinematics, namely, 3L2-3,GLb, which still achieves a high numerical accuracy for both transverse and in-plane stresses when compared to the kinematics that follow with even less DOFs. Most noteworthy, these results also demonstrate that RMVT-based LW plate elements with NDK and HLE combined are shown to be, in fact, insensitive to shear-locking, regardless of the global–local or standard approach considered in the stress analysis of the composite laminates, even especially thin with $a/h = 100$.

Additionally, to provide a more detailed description of the global–local stress analysis of the composite laminates (0°/90°/0°), with $a/h = 4$, 10 and 100, under a bi-sinusoidal load, Fig. 9 shows the through-thickness distributions of both displacements and stresses by RMVT-based LW plate elements using NDK according to the optimal global–local approach identified for each composite laminate, in line with its side-to-thickness ratio. As plainly evident from Fig. 9, the through-thickness distributions predicted demonstrate again a high level of numerical accuracy, in absolute agreement

with the 3D exact solutions, which holds for all side-to-thickness ratios from thick to thin composite laminates.

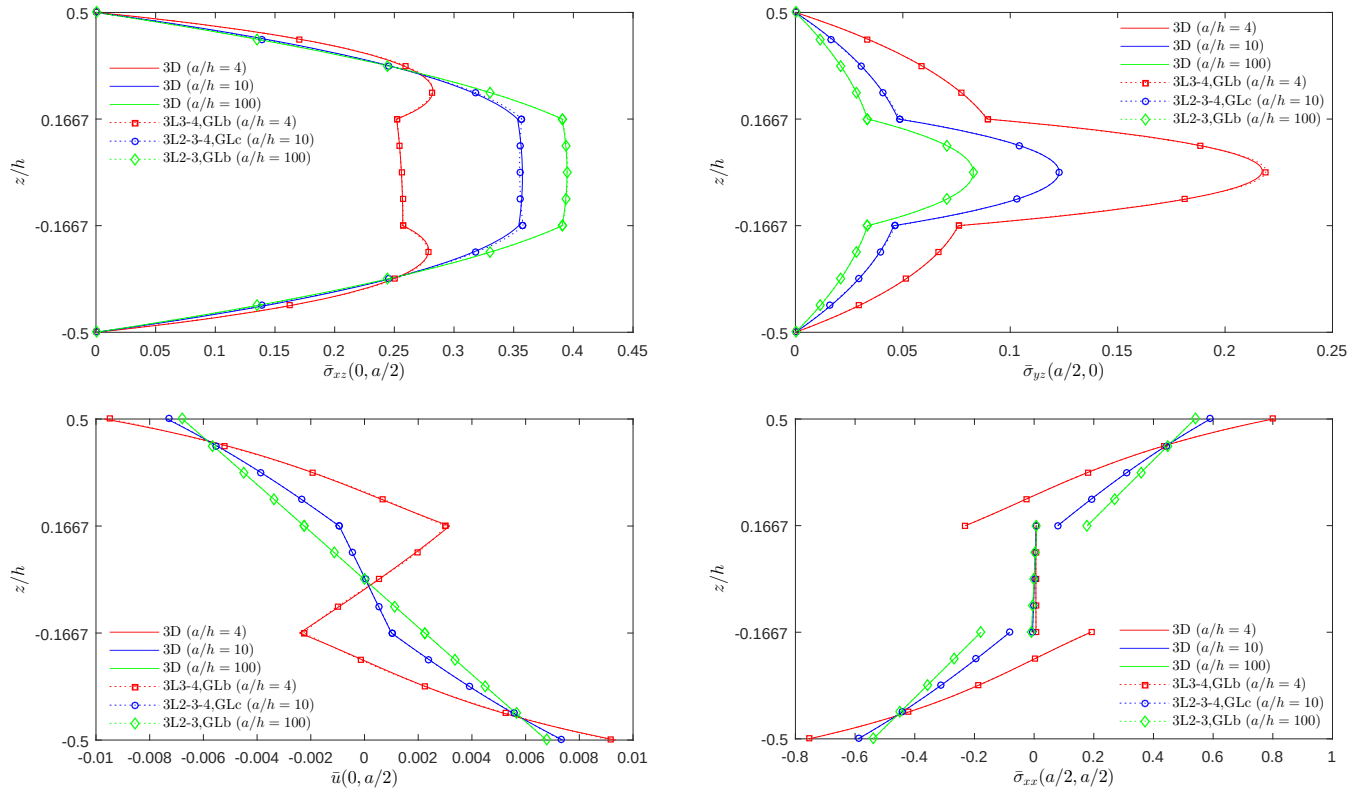

Figure 9: Composite laminates $(0°/90°/0°)$ under a bi-sinusoidal load ($a/h = 4, 10, 100$): through-thickness distributions by RMVT-based LW plate elements using NDK for a global–local analysis, alongside 3D exact solutions as derived from the work by Moleiro et al. [43].

7.3. Benchmark 3: composite laminates under a localized uniform load

Considering last the stress analysis of the simply supported square composite laminates $(0°/90°/0°)$ and $(0°/90°)_2$, with $a/h = 10$, under a localized uniform load, applied on a square region of side $a/5$ centred on the plate top surface, the following load and boundary conditions are used in practice, which do take advantage of the problem symmetries for computational efficiency, involving only a quarter of the plate, i.e. $(x, y) \in [0, a/2]$:

Localized uniform load

$$p(x, y) = -p_0, \quad \text{if } (x, y) \in [\tfrac{2a}{5}, \tfrac{a}{2}] \tag{39}$$

Boundary conditions

$$\begin{aligned} &\text{At } x = 0: \quad v = w = 0; \quad \text{At } x = \tfrac{a}{2}: \quad u = 0 \\ &\text{At } y = 0: \quad u = w = 0; \quad \text{At } y = \tfrac{a}{2}: \quad v = 0 \\ &\text{At } z = -\tfrac{h}{2}: \quad \sigma_{zz} = \sigma_{xz} = \sigma_{yz} = 0 \\ &\text{At } z = \tfrac{h}{2}: \quad \sigma_{xz} = \sigma_{yz} = 0 \end{aligned} \tag{40}$$

where $a = 0.1$ m and $p_0 = 1$ MPa, in agreement with the 3D exact solutions provided by Biscani et al. [34].

Since only a quarter of the plate is considered, besides simply supported conditions on the plate edges $x = y = 0$, symmetry conditions on the plate axes $x = y = a/2$ are employed, along with the real traction free boundary conditions on the plate top and bottom surfaces that can also be accurately imposed, as a benefit of RMVT-based elements.

In light of the localized uniform load, three different meshes are considered with increasing refinement in the loaded region by a standard h-refinement approach, denoted simply as mesh 5×5, 6×6 or 7×7 (though not all equally spaced), as depicted in Fig. 10. In fact, p-refinement is also considered by using either HLE4 or HLE5 in the mesh, although the computational efficiency of HLE4 is expected to be preferable.

Hence, the global–local stress analysis of the square composite laminates $(0°/90°/0°)$ and $(0°/90°)_2$, with $a/h = 10$, under a localized uniform load, by RMVT-based LW plate elements with NDK is prepared such that all three meshes can be used in combination with the same pre-established global–local regions. To be clear, these global–local regions with different degrees of kinematic refinement assigned locally to the desired nodes of RMVT-based LW plate elements are also depicted in Fig. 10. In essence, two different global–local approaches can be considered based on the pre-established global–local regions, namely, GLa or GLb, with a higher-degree of kinematic refinement towards the loaded region in the centre of the laminate, thus in the corner of the quarter plate model.

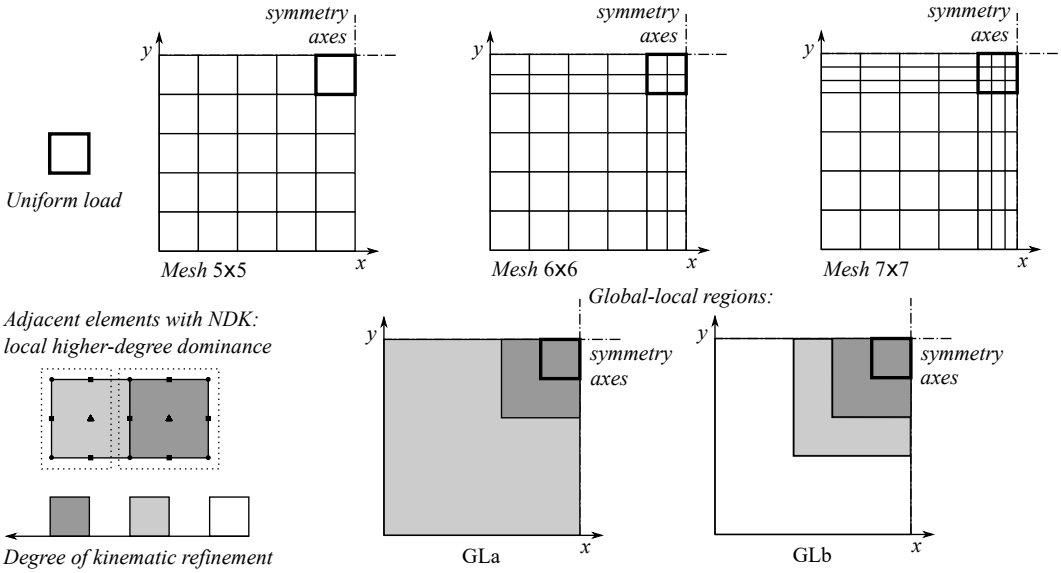

Figure 10: Global-local regions of RMVT-based LW plate elements with NDK, namely, GLa or GLb, as considered in every mesh for a global–local analysis of the composite laminates $(0°/90°/0°)$ and $(0°/90°)_2$ under a localized uniform load $(a/h = 10)$.

Subsequently, the results of the intended stress analysis of the square composite laminates $(0°/90°/0°)$ and $(0°/90°)_2$, with $a/h = 10$, under a localized uniform load, by RMVT-based LW plate elements, with or without the use of NDK for a global–local analysis, are now summarized in Table 8 and Table 9, respectively.

Table 8: Composite laminate $(0°/90°/0°)$ under a localized uniform load $(a/h = 10)$: displacements and stresses by RMVT-based LW plate elements with or without the use of NDK for a global–local analysis.

Mesh ⊥ Kinematics	$-10^5 w$[m] $(\frac{a}{2}, \frac{a}{2}, 0)$	σ_{xx}[MPa] $(\frac{a}{2}, \frac{a}{2}, -\frac{h}{2})$	σ_{xx}[MPa] $(\frac{a}{2}, \frac{a}{2}, \frac{h}{2})$	σ_{yy}[MPa] $(\frac{a}{2}, \frac{a}{2}, -\frac{h}{2})$	σ_{yy}[MPa] $(\frac{a}{2}, \frac{a}{2}, \frac{h}{2})$	$-10\sigma_{xz}$[MPa] $(\frac{5a}{12}, \frac{a}{2}, 0)$	$-10\sigma_{yz}$[MPa] $(\frac{a}{2}, \frac{5a}{12}, 0)$	$-\sigma_{zz}$[MPa] $(\frac{a}{2}, \frac{a}{2}, \frac{h}{2})$	DOFs
3D [34]	1.674	11.94		2.019		6.524		1.0	
7×7 HLE4 ⊥ 3L4	1.707	11.942	−12.276	2.021	−2.461	6.540	7.013	0.999	35022
7×7 HLE4 ⊥ 3L3-4,GLa	1.707	11.942	−12.277	2.021	−2.461	6.540	7.013	0.999	29838
7×7 HLE4 ⊥ 3L2-3-4,GLb	1.707	11.942	−12.277	2.021	−2.461	6.540	7.013	0.999	26094
6×6 HLE4 ⊥ 3L4	1.707	11.941	−12.268	2.019	−2.443	6.522	6.976	0.965	26286
6×6 HLE4 ⊥ 3L3-4,GLa	1.707	11.941	−12.268	2.019	−2.443	6.522	6.976	0.965	21966
6×6 HLE4 ⊥ 3L2-3-4,GLb$^{\triangleright}$	1.707	11.941	−12.268	2.019	−2.443	6.522	6.976	0.965	$^{\triangleright}$18798
5×5 HLE4 ⊥ 3L5	1.707	11.893	−12.382	2.005	−2.408	6.506	6.924	0.838	23136
5×5 HLE4 ⊥ 3L4	1.707	11.900	−12.327	2.004	−2.409	6.504	6.929	0.823	18798
6×6 HLE5 ⊥ 3L4	1.707	11.943	−12.264	2.021	−2.443	6.528	6.987	0.976	38454
5×5 HLE5 ⊥ 3L5	1.707	11.950	−12.243	2.022	−2.455	6.525	6.971	1.104	33696
5×5 HLE5 ⊥ 3L4	1.710	11.944	−12.317	2.031	−2.457	6.511	6.978	1.111	27378

$^{\triangleright}$ Selection of GL approach using NDK for optimal high numerical accuracy and computational efficiency.

A careful discussion of the results gathered in Tables 8–9 requires focusing on the mesh itself and on the kinematics, separately at first. In each table, the comparison between pairs of results that differ only on whether HLE4 or HLE5 are used in the mesh, 5×5 or 6×6, under the same kinematic assumptions in a standard approach, shows quite clearly that HLE5 can slightly improve the accuracy of the results, though involving much higher computational efforts, which can be reasonably avoided by a proper global–local approach using HLE4 instead. Hence, much like in the previous benchmarks, the numerical accuracy provided by HLE4, involving fewer DOFs than HLE5, seems to be preferable for computational efficiency. Moreover, the h-refinement provided by the meshes 5×5, 6×6 and 7×7 using HLE4, reveals, in fact, that the

Table 9: Composite laminate $(0°/90°)_2$ under a localized uniform load ($a/h = 10$): displacements and stresses by RMVT-based LW plate elements with or without the use of NDK for a global–local analysis.

Mesh ⊥ Kinematics	$-10^5 w$[m] $(\frac{a}{2}, \frac{a}{2}, 0)$	σ_{xx}[MPa] $(\frac{a}{2}, \frac{a}{2}, -\frac{h}{2})$	σ_{xx}[MPa] $(\frac{a}{2}, \frac{a}{2}, \frac{h}{2})$	σ_{yy}[MPa] $(\frac{a}{2}, \frac{a}{2}, -\frac{h}{2})$	σ_{yy}[MPa] $(\frac{a}{2}, \frac{a}{2}, \frac{h}{2})$	$-10\sigma_{xz}$[MPa] $(\frac{5a}{12}, \frac{a}{2}, 0)$	$-10\sigma_{yz}$[MPa] $(\frac{a}{2}, \frac{5a}{12}, 0)$	$-\sigma_{zz}$[MPa] $(\frac{a}{2}, \frac{a}{2}, \frac{h}{2})$	DOFs
3D [34]	1.719	11.28		1.823		6.104		1.0	
7×7 HLE4 ⊥ 4L4	1.749	11.297	−2.287	1.830	−11.530	6.141	6.958	0.999	45798
7×7 HLE4 ⊥ 4L3-4,GLa	1.748	11.286	−2.286	1.823	−11.541	6.144	6.970	0.999	38886
7×7 HLE4 ⊥ 4L2-3-4,GLb	1.748	11.286	−2.286	1.823	−11.541	6.144	6.970	0.999	33894
6×6 HLE4 ⊥ 4L4	1.749	11.598	−2.123	2.485	−11.929	6.203	7.285	0.987	34374
6×6 HLE4 ⊥ 4L3-4,GLa	1.748	11.284	−2.268	1.822	−11.538	6.112	6.940	0.965	28614
6×6 HLE4 ⊥ 4L2-3-4,GLb▷	1.748	11.284	−2.268	1.822	−11.538	6.112	6.940	0.965	▷24390
5×5 HLE4 ⊥ 4L5	1.748	11.240	−2.223	1.815	−11.688	6.073	6.937	0.847	30366
5×5 HLE4 ⊥ 4L4	1.748	11.240	−2.223	1.813	−11.652	6.076	6.921	0.834	24582
6×6 HLE5 ⊥ 4L4	1.748	11.288	−2.269	1.824	−11.532	6.127	6.951	0.976	50286
5×5 HLE5 ⊥ 4L5	1.748	11.288	−2.278	1.824	−11.462	6.107	6.959	1.095	44226
5×5 HLE5 ⊥ 4L4	1.750	11.108	−2.273	1.741	−11.531	6.092	6.943	1.107	35802

▷ Selection of GL approach using NDK for optimal high numerical accuracy and computational efficiency.

mesh 5×5 HLE4 is not sufficient to ensure converged results for the stresses, though the displacements already appear converged. Thus, leading to either a mesh 6×6 HLE4 or a mesh 7×7 HLE4. Examining now the kinematics, Tables 8–9 show that compared to the most computationally demanding standard approach, under equal kinematic assumptions, namely, 3L4 or 4L4 for each composite laminate, the selection of the optimal global–local approach, which ensures exactly the same high level of numerical accuracy, while involving the lowest number of DOFs, seems to rest on the kinematics 3L2-3-4,GLb or 4L2-3-4,GLb for each composite laminate, whether a mesh 6×6 HLE4 or 7×7 HLE4 is considered. Still, the increase in computational efforts by the mesh 7×7 HLE4 seems not to justify the slight improvement of the accuracy of the results, compared to the mesh 6×6 HLE4. Therefore, to ensure a high numerical accuracy and computational efficiency, all together, a mesh 6×6 HLE4 combined with the optimal global–local approach by the kinematics 3L2-3-4,GLb or 4L2-3-4,GLb for each composite laminate, seems to be the most suitable procedure.

Accordingly, a more insightful description of the global–local stress analysis of the composite laminates $(0°/90°/0°)$ and $(0°/90°)_2$, with $a/h = 10$, under a localized uniform load, by RMVT-based LW plate elements using NDK throughout the mesh, is provided by Fig. 11, showing contour distributions of transverse stresses, as set by the mesh 6×6 HLE4 and the optimal global–local approach, namely, 3L2-3-4,GLb or 4L2-3-4,GLb for each composite laminate, respectively.

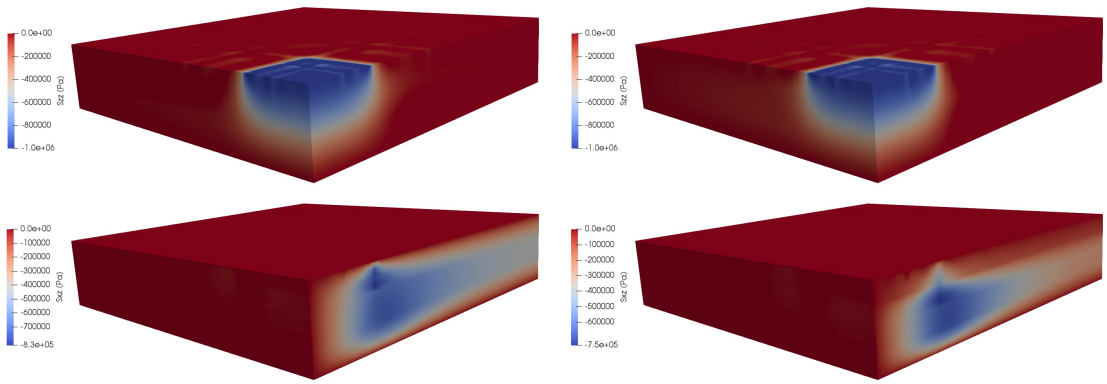

Figure 11: Composite laminates $(0°/90°/0°)$ and $(0°/90°)_2$ under a localized uniform load ($a/h = 10$): transverse stresses distributions by RMVT-based LW plate elements using NDK for a global–local analysis, i.e. 3L2-3-4,GLb (on the left) and 4L2-3-4,GLb (on the right), respectively.

As perfectly clear from Fig. 11, in spite of the strong localized effects on the stress field nearby the loaded region, the solution of the global–local stress analysis by RMVT-based LW plate elements using NDK can actually achieve quite a high numerical accuracy, locally, while maintaining the quality of the numerical results in the transitional and global regions, as long as the different degrees of kinematic refinement are pre-established throughout the mesh in a gradual form. In fact, if employed properly, the use of NDK capabilities seems to safeguard the quality of the numerical results everywhere in the mesh, even in the presence of such strong localized effects.

Furthermore, to complete in greater detail the global–local stress analysis of the composite laminates $(0°/90°/0°)$ and $(0°/90°)_2$, with $a/h = 10$, under a localized uniform load, Fig. 12 shows the through-thickness distributions of both

transverse and in-plane stresses by RMVT-based LW plate elements using NDK, as set by the mesh 6×6 HLE4 and the optimal global–local approach, namely, 3L2-3-4,GLb or 4L2-3-4,GLb for each composite laminate, respectively.

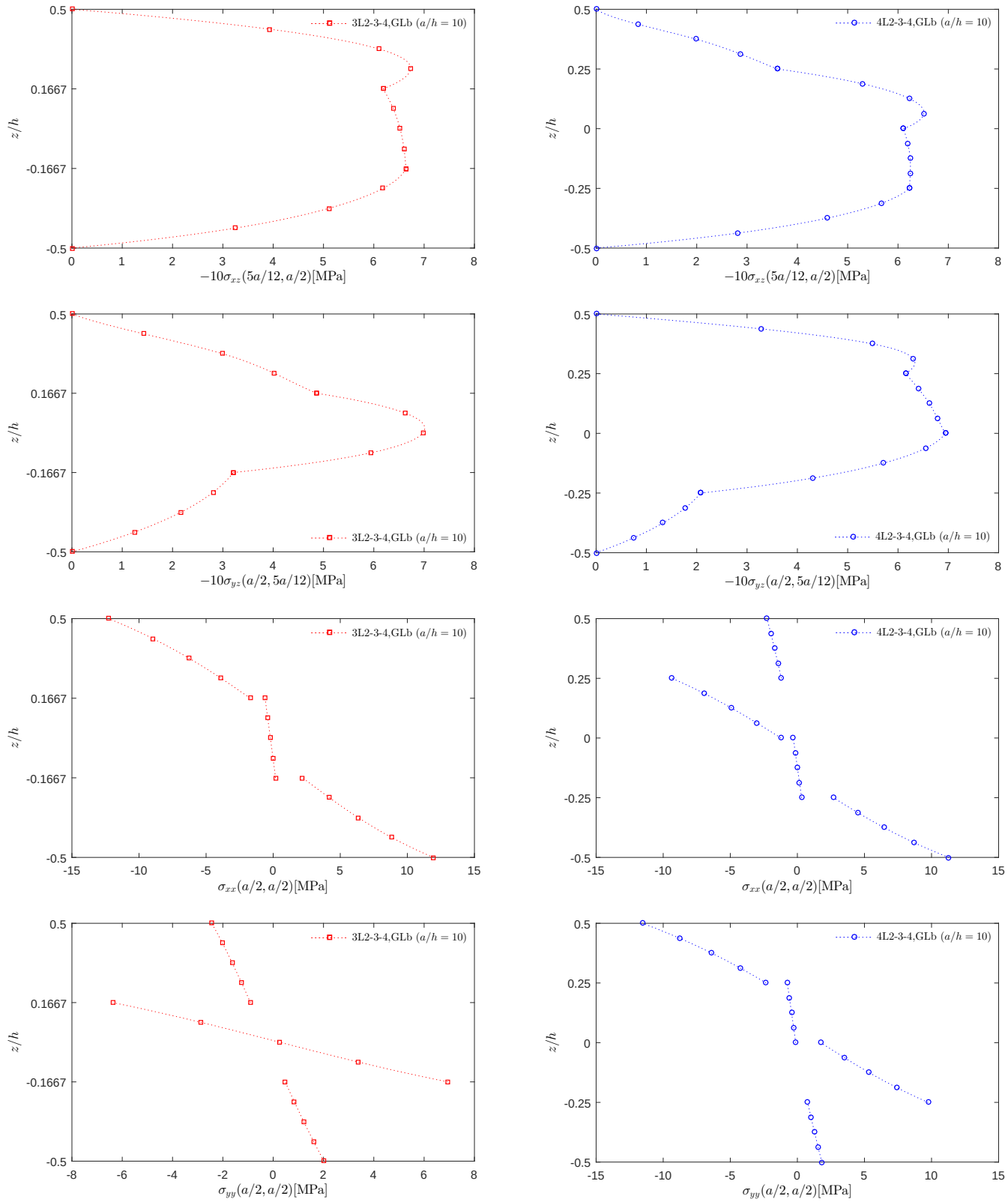

Figure 12: Composite laminates $(0°/90°/0°)$ and $(0°/90°)_2$ under a localized uniform load $(a/h = 10)$: through-thickness distributions by RMVT-based LW plate elements using NDK for a global–local analysis.

8. Conclusions

In light of the ever-growing demands on the modelling of multilayered composite structures to capture complicated local effects with high numerical accuracy, all along maintaining computational efficient techniques, new layerwise (LW) finite elements based on Reissner's Mixed Variational Theorem (RMVT) are proposed, with node-dependent kinematics (NDK) capabilities, in the framework of Carrera Unified Formulation (CUF), especially designed for global–local stress analysis of multilayered plates. In fact, as originally introduced to develop 2D models, CUF can conveniently incorporate any degree of kinematic refinement, as appropriate, using the so-called thickness functions in a unified compact form. The ensuing technique of NDK relies on a novel advanced approach. The degree of kinematic refinement, which usually holds equally for the entire element, can be taken a step further, by being assigned locally to each of its nodes, making full use of CUF to render NDK capabilities to the elements. Owing to this novel approach, elements with NDK capabilities can be applied throughout the entire mesh, adjusting the degree of kinematic refinement locally on the desired nodes, as necessary, without changing the mesh itself, bypassing *ad hoc* procedures to couple kinematically different models. In addition, even though the elements can adopt any type of nodal shape functions, high p-order hierarchical Legendre expansions (HLE) can also be combined with NDK, achieving excellent convergence rates. These capabilities combined, explored first under the Principal of Virtual Displacements (PVD), are here first-ever integrated in the proposed elements under RMVT, which is shown to be most beneficial for an accurate stress analysis.

The predictive capabilities of the proposed RMVT-based LW plate elements with NDK, involving high p-order (1D) Legendre thickness functions, to incorporate any degree of kinematic refinement as appropriate using CUF, combined with high p-order (2D) HLE, are demonstrated through a set of numerical results. The focus is on stress analysis of various multilayered composite plates, with different side-to-thickness ratios from thick to thin laminates, under distinct loading conditions, including local effects, considering well-known benchmark 3D exact solutions for assessment. A series of global–local approaches are investigated for each benchmark, applying the proposed RMVT-based LW plate elements with NDK throughout the entire mesh, adapting to local, transitional and global regions straightforwardly, providing high numerical accuracy, locally, in perfect agreement with the 3D exact solutions, with minimal computational efforts, globally. Moreover, RMVT-based LW plate elements with NDK and HLE combined are shown to be, in fact, insensitive to shear-locking, regardless of the global–local or standard approach considered in the stress analysis of multilayered composite plates. Furthermore, the added NDK capabilities designed for global–local analysis can evidently reduce the computational efforts substantially, capturing local effects accurately, while preserving the quality of the solution in the transitional and global regions. Ultimately, this computational efficiency ensured by NKD can be even more amplified in large size problems.

Acknowledgements

The first author acknowledges the financial support received through National Funds from "Fundação para a Ciência e a Tecnologia" (FCT) via IDMEC, under the Associated Laboratory of Energy, Transports and Aeronautics (LAETA), Project UID/EMS/50022/2019, as well as inter-institutional projects funds from LAETA. In addition, the first author also thanks FCT for the Sabbatical Leave Grant SFRH/BSAB/143061/2018.

Appendix A

The explicit expressions of each *Fundamental Nuclei* (FN) of the RMVT-based LW plate elements with NDK, namely, $\boldsymbol{K}_{uu}^{ks\tau ji}$, $\boldsymbol{K}_{u\sigma}^{ks\tau ji}$, $\boldsymbol{K}_{\sigma u}^{ks\tau ji}$ and $\boldsymbol{K}_{\sigma\sigma}^{ks\tau ji}$, of size 3×3 each one, are here presented in compact form first, as follows:

$$\boldsymbol{K}_{uu}^{ks\tau ji} = \int_\Omega \boldsymbol{D}_p^{\intercal}(N_j\boldsymbol{I})\hat{\boldsymbol{C}}_{pp}^{k}\left[\int_{h^k}(F_s^{jk}F_\tau^{ik}\boldsymbol{I})\,\mathrm{d}h^k\right]\boldsymbol{D}_p(N_i\boldsymbol{I})\,\mathrm{d}\Omega \tag{A.1}$$

$$\begin{aligned}\boldsymbol{K}_{u\sigma}^{ks\tau ji} = {}& \int_\Omega \boldsymbol{D}_p^{\intercal}(N_j\boldsymbol{I})\hat{\boldsymbol{C}}_{pn}^{k}\left[\int_{h^k}(F_s^{jk}F_\tau^{ik}\boldsymbol{I})\,\mathrm{d}h^k\right](N_i\boldsymbol{I})\,\mathrm{d}\Omega \\ & + \int_\Omega \boldsymbol{D}_{np}^{\intercal}(N_j\boldsymbol{I})\left[\int_{h^k}(F_s^{jk}F_\tau^{ik}\boldsymbol{I})\,\mathrm{d}h^k\right](N_i\boldsymbol{I})\,\mathrm{d}\Omega \\ & + \int_\Omega (N_j\boldsymbol{I})\left[\int_{h^k}\boldsymbol{D}_{nz}^{\intercal}(F_s^{jk}\boldsymbol{I})(F_\tau^{ik}\boldsymbol{I})\,\mathrm{d}h^k\right](N_i\boldsymbol{I})\,\mathrm{d}\Omega\end{aligned} \tag{A.2}$$

$$\begin{aligned}\boldsymbol{K}_{\sigma u}^{ks\tau ji} = {}& \int_\Omega (N_j\boldsymbol{I})\left[\int_{h^k}(F_s^{jk}F_\tau^{ik}\boldsymbol{I})\,\mathrm{d}h^k\right]\boldsymbol{D}_{np}(N_i\boldsymbol{I})\,\mathrm{d}\Omega \\ & + \int_\Omega (N_j\boldsymbol{I})\left[\int_{h^k}(F_s^{jk}\boldsymbol{I})\boldsymbol{D}_{nz}(F_\tau^{ik}\boldsymbol{I})\,\mathrm{d}h^k\right](N_i\boldsymbol{I})\,\mathrm{d}\Omega \\ & - \int_\Omega (N_j\boldsymbol{I})\hat{\boldsymbol{C}}_{np}^{k}\left[\int_{h^k}(F_s^{jk}F_\tau^{ik}\boldsymbol{I})\,\mathrm{d}h^k\right]\boldsymbol{D}_p(N_i\boldsymbol{I})\,\mathrm{d}\Omega\end{aligned} \tag{A.3}$$

$$\boldsymbol{K}_{\sigma\sigma}^{ks\tau ji} = -\int_\Omega (N_j\boldsymbol{I})\hat{\boldsymbol{C}}_{nn}^{k}\left[\int_{h^k}(F_s^{jk}F_\tau^{ik}\boldsymbol{I})\,\mathrm{d}h^k\right](N_i\boldsymbol{I})\,\mathrm{d}\Omega \tag{A.4}$$

where all possible non-zero coefficients in the matrices $\hat{\boldsymbol{C}}^k_{pp}$, $\hat{\boldsymbol{C}}^k_{pn}$, $\hat{\boldsymbol{C}}^k_{np}$ and $\hat{\boldsymbol{C}}^k_{nn}$ are as shown:

$$\begin{aligned}
\hat{\boldsymbol{C}}^k_{pp} &= \begin{bmatrix} \hat{C}^k_{11} & \hat{C}^k_{12} & \hat{C}^k_{16} \\ \hat{C}^k_{12} & \hat{C}^k_{22} & \hat{C}^k_{26} \\ \hat{C}^k_{16} & \hat{C}^k_{26} & \hat{C}^k_{66} \end{bmatrix}, \hat{\boldsymbol{C}}^k_{pn} = \begin{bmatrix} \hat{C}^k_{13} & 0 & 0 \\ \hat{C}^k_{23} & 0 & 0 \\ \hat{C}^k_{36} & 0 & 0 \end{bmatrix} \\
\hat{\boldsymbol{C}}^k_{nn} &= \begin{bmatrix} \hat{C}^k_{33} & 0 & 0 \\ 0 & \hat{C}^k_{55} & \hat{C}^k_{45} \\ 0 & \hat{C}^k_{45} & \hat{C}^k_{44} \end{bmatrix}, \hat{\boldsymbol{C}}^k_{np} = -\hat{\boldsymbol{C}}^{k\,\intercal}_{pn}
\end{aligned} \tag{A.5}$$

Accordingly, the explicit expressions of each FN in expanded form are also presented, i.e. all 9 components of each FN, involving the standard comma derivative notation for brevity, as follows:

$$\begin{aligned}
\boldsymbol{K}^{ks\tau ji}_{uu\,11} = {} & \hat{C}^k_{11} \left[\int_{h^k} F^{jk}_s F^{ik}_\tau \,\mathrm{d}h^k\right] \int_\Omega N_{j,x} N_{i,x} \,\mathrm{d}\Omega \\
& + \hat{C}^k_{16} \left[\int_{h^k} F^{jk}_s F^{ik}_\tau \,\mathrm{d}h^k\right] \int_\Omega N_{j,y} N_{i,x} \,\mathrm{d}\Omega \\
& + \hat{C}^k_{16} \left[\int_{h^k} F^{jk}_s F^{ik}_\tau \,\mathrm{d}h^k\right] \int_\Omega N_{j,x} N_{i,y} \,\mathrm{d}\Omega \\
& + \hat{C}^k_{66} \left[\int_{h^k} F^{jk}_s F^{ik}_\tau \,\mathrm{d}h^k\right] \int_\Omega N_{j,y} N_{i,y} \,\mathrm{d}\Omega
\end{aligned} \tag{A.6}$$

$$\begin{aligned}
\boldsymbol{K}^{ks\tau ji}_{uu\,12} = {} & \hat{C}^k_{16} \left[\int_{h^k} F^{jk}_s F^{ik}_\tau \,\mathrm{d}h^k\right] \int_\Omega N_{j,x} N_{i,x} \,\mathrm{d}\Omega \\
& + \hat{C}^k_{66} \left[\int_{h^k} F^{jk}_s F^{ik}_\tau \,\mathrm{d}h^k\right] \int_\Omega N_{j,y} N_{i,x} \,\mathrm{d}\Omega \\
& + \hat{C}^k_{12} \left[\int_{h^k} F^{jk}_s F^{ik}_\tau \,\mathrm{d}h^k\right] \int_\Omega N_{j,x} N_{i,y} \,\mathrm{d}\Omega \\
& + \hat{C}^k_{26} \left[\int_{h^k} F^{jk}_s F^{ik}_\tau \,\mathrm{d}h^k\right] \int_\Omega N_{j,y} N_{i,y} \,\mathrm{d}\Omega
\end{aligned} \tag{A.7}$$

$$\boldsymbol{K}^{ks\tau ji}_{uu\,13} = 0 \tag{A.8}$$

$$\begin{aligned}
\boldsymbol{K}^{ks\tau ji}_{uu\,21} = {} & \hat{C}^k_{16} \left[\int_{h^k} F^{jk}_s F^{ik}_\tau \,\mathrm{d}h^k\right] \int_\Omega N_{j,x} N_{i,x} \,\mathrm{d}\Omega \\
& + \hat{C}^k_{12} \left[\int_{h^k} F^{jk}_s F^{ik}_\tau \,\mathrm{d}h^k\right] \int_\Omega N_{j,y} N_{i,x} \,\mathrm{d}\Omega \\
& + \hat{C}^k_{66} \left[\int_{h^k} F^{jk}_s F^{ik}_\tau \,\mathrm{d}h^k\right] \int_\Omega N_{j,x} N_{i,y} \,\mathrm{d}\Omega \\
& + \hat{C}^k_{26} \left[\int_{h^k} F^{jk}_s F^{ik}_\tau \,\mathrm{d}h^k\right] \int_\Omega N_{j,y} N_{i,y} \,\mathrm{d}\Omega
\end{aligned} \tag{A.9}$$

$$\begin{aligned}
\boldsymbol{K}^{ks\tau ji}_{uu\,22} = {} & \hat{C}^k_{66} \left[\int_{h^k} F^{jk}_s F^{ik}_\tau \,\mathrm{d}h^k\right] \int_\Omega N_{j,x} N_{i,x} \,\mathrm{d}\Omega \\
& + \hat{C}^k_{26} \left[\int_{h^k} F^{jk}_s F^{ik}_\tau \,\mathrm{d}h^k\right] \int_\Omega N_{j,y} N_{i,x} \,\mathrm{d}\Omega \\
& + \hat{C}^k_{26} \left[\int_{h^k} F^{jk}_s F^{ik}_\tau \,\mathrm{d}h^k\right] \int_\Omega N_{j,x} N_{i,y} \,\mathrm{d}\Omega \\
& + \hat{C}^k_{22} \left[\int_{h^k} F^{jk}_s F^{ik}_\tau \,\mathrm{d}h^k\right] \int_\Omega N_{j,y} N_{i,y} \,\mathrm{d}\Omega
\end{aligned} \tag{A.10}$$

$$\boldsymbol{K}^{ks\tau ji}_{uu\,23} = 0 \tag{A.11}$$

$$\boldsymbol{K}^{ks\tau ji}_{uu\,31} = 0 \tag{A.12}$$

$$\boldsymbol{K}^{ks\tau ji}_{uu\,32} = 0 \tag{A.13}$$

$$\boldsymbol{K}^{ks\tau ji}_{uu\,33} = 0 \tag{A.14}$$

$$\begin{aligned}
\boldsymbol{K}^{ks\tau ji}_{u\sigma\,11} = {} & \hat{C}^k_{13} \left[\int_{h^k} F^{jk}_s F^{ik}_\tau \,\mathrm{d}h^k\right] \int_\Omega N_{j,x} N_i \,\mathrm{d}\Omega \\
& + \hat{C}^k_{36} \left[\int_{h^k} F^{jk}_s F^{ik}_\tau \,\mathrm{d}h^k\right] \int_\Omega N_{j,y} N_i \,\mathrm{d}\Omega
\end{aligned} \tag{A.15}$$

$$\boldsymbol{K}^{ks\tau ji}_{u\sigma\,12} = \left[\int_{h^k} F^{jk}_{s,z} F^{ik}_\tau \,\mathrm{d}h^k\right] \int_\Omega N_j N_i \,\mathrm{d}\Omega \tag{A.16}$$

$$\boldsymbol{K}^{ks\tau ji}_{u\sigma\,13} = 0 \tag{A.17}$$

$$\begin{aligned}
\boldsymbol{K}^{ks\tau ji}_{u\sigma\,21} = {} & \hat{C}^k_{36} \left[\int_{h^k} F^{jk}_s F^{ik}_\tau \,\mathrm{d}h^k\right] \int_\Omega N_{j,x} N_i \,\mathrm{d}\Omega \\
& + \hat{C}^k_{23} \left[\int_{h^k} F^{jk}_s F^{ik}_\tau \,\mathrm{d}h^k\right] \int_\Omega N_{j,y} N_i \,\mathrm{d}\Omega
\end{aligned} \tag{A.18}$$

$$\boldsymbol{K}^{ks\tau ji}_{u\sigma\,22} = 0 \tag{A.19}$$

$$\boldsymbol{K}^{ks\tau ji}_{u\sigma\,23} = \left[\int_{h^k} F^{jk}_{s,z} F^{ik}_{\tau}\,\mathrm{d}h^k\right] \int_\Omega N_j N_i\,\mathrm{d}\Omega \tag{A.20}$$

$$\boldsymbol{K}^{ks\tau ji}_{u\sigma\,31} = \left[\int_{h^k} F^{jk}_{s,z} F^{ik}_{\tau}\,\mathrm{d}h^k\right] \int_\Omega N_j N_i\,\mathrm{d}\Omega \tag{A.21}$$

$$\boldsymbol{K}^{ks\tau ji}_{u\sigma\,32} = \left[\int_{h^k} F^{jk}_{s} F^{ik}_{\tau}\,\mathrm{d}h^k\right] \int_\Omega N_{j,x} N_i\,\mathrm{d}\Omega \tag{A.22}$$

$$\boldsymbol{K}^{ks\tau ji}_{u\sigma\,33} = \left[\int_{h^k} F^{jk}_{s} F^{ik}_{\tau}\,\mathrm{d}h^k\right] \int_\Omega N_{j,y} N_i\,\mathrm{d}\Omega \tag{A.23}$$

$$\boldsymbol{K}^{ks\tau ji}_{\sigma u\,11} = 0 \tag{A.24}$$

$$\boldsymbol{K}^{ks\tau ji}_{\sigma u\,12} = 0 \tag{A.25}$$

$$\boldsymbol{K}^{ks\tau ji}_{\sigma u\,13} = \left[\int_{h^k} F^{jk}_{s} F^{ik}_{\tau,z}\,\mathrm{d}h^k\right] \int_\Omega N_j N_i\,\mathrm{d}\Omega \tag{A.26}$$

$$\boldsymbol{K}^{ks\tau ji}_{\sigma u\,21} = \left[\int_{h^k} F^{jk}_{s} F^{ik}_{\tau,z}\,\mathrm{d}h^k\right] \int_\Omega N_j N_i\,\mathrm{d}\Omega \tag{A.27}$$

$$\boldsymbol{K}^{ks\tau ji}_{\sigma u\,22} = 0 \tag{A.28}$$

$$\boldsymbol{K}^{ks\tau ji}_{\sigma u\,23} = \left[\int_{h^k} F^{jk}_{s} F^{ik}_{\tau}\,\mathrm{d}h^k\right] \int_\Omega N_j N_{i,x}\,\mathrm{d}\Omega \tag{A.29}$$

$$\begin{aligned}\boldsymbol{K}^{ks\tau ji}_{\sigma u\,31} = {} & \hat{C}^k_{13} \left[\int_{h^k} F^{jk}_{s} F^{ik}_{\tau}\,\mathrm{d}h^k\right] \int_\Omega N_j N_{i,x}\,\mathrm{d}\Omega \\ & + \hat{C}^k_{36} \left[\int_{h^k} F^{jk}_{s} F^{ik}_{\tau}\,\mathrm{d}h^k\right] \int_\Omega N_j N_{i,y}\,\mathrm{d}\Omega\end{aligned} \tag{A.30}$$

$$\begin{aligned}\boldsymbol{K}^{ks\tau ji}_{\sigma u\,32} = {} & \hat{C}^k_{36} \left[\int_{h^k} F^{jk}_{s} F^{ik}_{\tau}\,\mathrm{d}h^k\right] \int_\Omega N_j N_{i,x}\,\mathrm{d}\Omega \\ & + \hat{C}^k_{23} \left[\int_{h^k} F^{jk}_{s} F^{ik}_{\tau}\,\mathrm{d}h^k\right] \int_\Omega N_j N_{i,y}\,\mathrm{d}\Omega \\ & + \left[\int_{h^k} F^{jk}_{s} F^{ik}_{\tau,z}\,\mathrm{d}h^k\right] \int_\Omega N_j N_i\,\mathrm{d}\Omega\end{aligned} \tag{A.31}$$

$$\boldsymbol{K}^{ks\tau ji}_{\sigma u\,33} = \left[\int_{h^k} F^{jk}_{s} F^{ik}_{\tau}\,\mathrm{d}h^k\right] \int_\Omega N_j N_{i,y}\,\mathrm{d}\Omega \tag{A.32}$$

$$\boldsymbol{K}^{ks\tau ji}_{\sigma\sigma\,11} = -\hat{C}^k_{33} \left[\int_{h^k} F^{jk}_{s} F^{ik}_{\tau}\,\mathrm{d}h^k\right] \int_\Omega N_j N_i\,\mathrm{d}\Omega \tag{A.33}$$

$$\boldsymbol{K}^{ks\tau ji}_{\sigma\sigma\,12} = 0 \tag{A.34}$$

$$\boldsymbol{K}^{ks\tau ji}_{\sigma\sigma\,13} = 0 \tag{A.35}$$

$$\boldsymbol{K}^{ks\tau ji}_{\sigma\sigma\,21} = 0 \tag{A.36}$$

$$\boldsymbol{K}^{ks\tau ji}_{\sigma\sigma\,22} = -\hat{C}^k_{55} \left[\int_{h^k} F^{jk}_{s} F^{ik}_{\tau}\,\mathrm{d}h^k\right] \int_\Omega N_j N_i\,\mathrm{d}\Omega \tag{A.37}$$

$$\boldsymbol{K}^{ks\tau ji}_{\sigma\sigma\,23} = -\hat{C}^k_{45} \left[\int_{h^k} F^{jk}_{s} F^{ik}_{\tau}\,\mathrm{d}h^k\right] \int_\Omega N_j N_i\,\mathrm{d}\Omega \tag{A.38}$$

$$\boldsymbol{K}^{ks\tau ji}_{\sigma\sigma\,31} = 0 \tag{A.39}$$

$$\boldsymbol{K}^{ks\tau ji}_{\sigma\sigma\,32} = -\hat{C}^k_{45} \left[\int_{h^k} F^{jk}_{s} F^{ik}_{\tau}\,\mathrm{d}h^k\right] \int_\Omega N_j N_i\,\mathrm{d}\Omega \tag{A.40}$$

$$\boldsymbol{K}^{ks\tau ji}_{\sigma\sigma\,33} = -\hat{C}^k_{44} \left[\int_{h^k} F^{jk}_{s} F^{ik}_{\tau}\,\mathrm{d}h^k\right] \int_\Omega N_j N_i\,\mathrm{d}\Omega \tag{A.41}$$

Data availability

The raw/processed data required to reproduce these findings cannot be shared at this time as the data also forms part of an ongoing study.

References

[1] Reddy JN, Robbins Jr DH. Theories and computational models for composite laminates. Appl. Mech. Rev. 1994;47(6):147-169.

[2] Noor AK, Burton WS. Assessment of shear deformation theories for multilayered composite plates. Appl. Mech. Rev. 1989;42(1):1-13.

[3] Reddy JN. Mechanics of Laminated Composite Plates and Shells: Theory and Analysis. Boca Raton, Florida: CRC Press, 2004.

[4] Carrera E. Theories and finite elements for multilayered, anisotropic, composite plates and shells. Arch. Comput. Method Eng. 2002;9(2):87-140.

[5] Carrera E. Theories and finite elements for multilayered plates and shells: a unified compact formulation with numerical assessment and benchmarking. Arch. Comput. Method Eng. 2003;10(3):215-296.

[6] Noor AK, Burton WS. Computational models for high-temperature multilayered composite plates and shells. Appl. Mech. Rev. 1992;45(10):419-446.

[7] Tang YY, Noor AK, Xu K. Assessment of computational models for thermoelectroelastic multilayered plates. Comput. Struct. 1996;61(5):915-933.

[8] Saravanos DA, Heyliger PR. Mechanics and computational models for laminated piezoelectric beams, plates and shells. Appl. Mech. Rev. 1999;52(10):305-320.

[9] Benjeddou A. Advances in piezoelectric finite element modeling of adaptive structural elements: a survey. Comput. Struct. 2000;76:347-363.

[10] Carrera E, Cinefra M, Petrolo M, Zappino E. Finite element analysis of structures through unified formulation. Chichester, West Sussex: John Wiley & Sons, 2014.

[11] Carrera E. Developments, ideas, and evaluations based upon Reissner's Mixed Variational Theorem in the modeling of multilayered plates and shells. Appl. Mech. Rev. 2001;54(4):301-329.

[12] Carrera E, Demasi L. Classical and advanced multilayered plate elements based upon PVD and RMVT. Part 1: Derivation of finite element matrices. Int. J. Numer. Methods Eng. 2002;55:191-231.

[13] Carrera E, Demasi L. Classical and advanced multilayered plate elements based upon PVD and RMVT. Part 2: Numerical implementations. Int. J. Numer. Methods Eng. 2002;55:253-291.

[14] Carrera E, Boscolo M. Classical and mixed finite elements for static and dynamic analysis of piezoelectric plates. Int. J. Numer. Methods Eng. 2007;70:1135-1181.

[15] Cinefra M, Petrolo M, Li G, Carrera E. Hygrothermal analysis of multilayered composite plates by variable kinematic finite elements. J. Therm. Stresses 2017;40:1502-1522.

[16] Cinefra M, Petrolo M, Li G, Carrera E. Variable kinematic shell elements for composite laminates accounting for hygrothermal effects. J. Therm. Stresses 2017;40:1523-1544.

[17] de Miguel AG, Carrera E, Pagani A, Zappino E. Accurate evaluation of interlaminar stresses in composite laminates via mixed one-dimensional formulation. AIAA J. 2018;56(11):1-13.

[18] Babuška I, Szabó BA, Katz IN. The p-version of the finite element method. SIAM J. Numer. Anal. 1981;18(3):515-545.

[19] Szabó B, Düster A, Rank E. The p-version of the Finite Element Method. In: Stein E, de Borst R, Hughes TJR, editors. Encyclopedia of Computational Mechanics. Wiley Online Library, 2004. p. 119-139.

[20] Szabó B, Babuška I. Introduction to Finite Element Analysis: Formulation, Verification and Validation. Chichester, West Sussex: John Wiley & Sons, 2011.

[21] Pagani A, de Miguel A, Petrolo M, Carrera E. Analysis of laminated beams via Unified Formulation and Legendre polynomial expansions. Compos. Struct. 2016;156:78-92.

[22] Carrera E, de Miguel A, Pagani A. Hierarchical theories of structures based on Legendre polynomial expansions with finite element applications. Int. J. Mech. Sci. 2017;120:286-300.

[23] Moleiro F, Mota Soares CM, Mota Soares CA, Reddy JN. Layerwise mixed least-squares finite element models for static and free vibration analysis of multilayered composite plates. Compos. Struct. 2010;92(9):2328-2338.

[24] Moleiro F, Mota Soares CM, Mota Soares CA, Reddy JN. Layerwise mixed models for analysis of multilayered piezoelectric composite plates using least-squares formulation. Compos. Struct. 2015;119:134-149.

[25] Moleiro F, Franco Correia VM, Araújo AL, Mota Soares CM, Ferreira AJM, Reddy JN. Deformation and stresses of multilayered plates with embedded functionally graded material layers using a layerwise mixed model. Compos. Pt. B-Eng. 2019;156:274-291.

[26] Moleiro F, Franco Correia VM, Ferreira AJM, Reddy JN. Fully coupled thermo-mechanical analysis of multilayered plates with embedded FGM skins or core layers using a layerwise mixed model. Compos. Struct. 2019;210:971-996.

[27] Moleiro F, Carrera E, Li G, Cinefra M, Reddy JN. Hygro-thermo-mechanical modelling of multilayered plates: hybrid composite laminates, fibre metal laminates and sandwich plates. Compos. Pt. B-Eng. 2019;177:107388.

[28] Moleiro F, Carrera E, Ferreira AJM, Reddy JN. Hygro-thermo-mechanical modelling and analysis of multilayered plates with embedded functionally graded material layers. Compos. Struct. 2019, 111442, *In Press*, https://doi.org/10.1016/j.compstruct.2019.111442.

[29] Warburton TC, Sherwin SJ, Karniadakis GE. Basis functions for triangular and quadrilateral high-order elements. SIAM J. Sci. Comput. 1999;20(5):1671-1695.

[30] Fish J. The s-version of the finite element method. Comput. Struct. 1992;43(3):539-547.

[31] Blanco PJ, Feijóo RA, Urquiza SA. A variational approach for coupling kinematically incompatible structural models. Comput. Methods Appl. Mech. Eng. 2008;197(17):1577-1602.

[32] Blanco PJ, Feijóo RA. Sensitivity analysis in kinematically incompatible models. Comput. Methods Appl. Mech. Eng. 2009;198(41):3287-3298.

[33] Dhia HB, Rateau G. The Arlequin method as a flexible engineering design tool. Int. J. Numer. Methods Eng. 2005;62(11):1442-1462.

[34] Biscani F, Giunta G, Belouettar S, Carrera E, Hu H. Variable kinematic plate elements coupled via Arlequin method. Int. J. Numer. Methods Eng. 2012;91:1264-1290.

[35] Biscani F, Nali P, Belouettar S, Carrera E. Coupling of hierarchical piezoelectric plate finite elements via Arlequin method. J. Intell. Mater. Syst. Struct. 2012;23(7):749-764.

[36] Carrera E, Zappino E. One-dimensional finite element formulation with node-dependent kinematics. Comput. Struct. 2017;192:114-125.

[37] Carrera E, Zappino E, Li G. Finite element models with node-dependent kinematics for the analysis of composite beam structures. Compos. Pt. B-Eng. 2018;132:35-48.

[38] Carrera E, Pagani A, Valvano S. Multilayered plate elements accounting for refined theories and node-dependent kinematics. Compos. Pt. B-Eng. 2017;114:189-210.

[39] Zappino E, Li G, Pagani A, Carrera E. Global-local analysis of laminated plates by node-dependent kinematic finite elements with variable ESL/LW capabilities. Compos. Struct. 2017;172:1-14.

[40] Zappino E, Li G, Pagani A, Carrera E, de Miguel AG. Use of higher-order Legendre polynomials for multilayered plate elements with node-dependent kinematics. Compos. Struct. 2018;202:222-232.

[41] Pagano NJ. Exact solutions for composite laminates in cylindrical bending. J. Compos. Mater. 1969;3:398-411.

[42] Pagano NJ. Exact solutions for rectangular bidirectional composites and sandwich plates. J. Compos. Mater. 1970;4:20-34.

[43] Moleiro F, Mota Soares CM, Mota Soares CA, Reddy JN. Benchmark exact solutions for the static analysis of multilayered piezoelectric composite plates using PVDF. Compos. Struct. 2014;107:389-395.